Thermal Models of Electric Powertrain Components for Cooling System Simulation and Design Requirements

An Undergraduate Honors Thesis

Submitted to the Department of Mechanical Engineering

The Ohio State University

In Partial Fulfillment of the Requirements

For Graduation with Honors Research Distinction in Mechanical Engineering

Zachary Salyer

May 2019

Dr. Marcello Canova, Advisor

Abstract

The powertrain of a typical electric vehicle consists of a battery pack, an electric machine, a control system, and a cooling system. As these components operate, their inefficiencies generate heat that must be dissipated. In high-performance electric vehicles for racing applications, thermal limitations in the electric machine or the motor controller could significantly reduce the power output of the motorcycle. To prevent thermal limitations, simulations using thermal models must be performed to determine the cooling system specifications required.

The purpose of this research is to develop a thermal model of Buckeye Current's electric powertrain and determine cooling system requirements based on the power demand of the Isle of Man TT Zero from a full-vehicle simulation.

Physics based thermal models of the components have been developed and implemented in Simulink, then integrated with the simulation software already developed by the Buckeye Current team for race performance prediction. An initial calibration of the model parameters was conducted using data from the Pikes Peak International Hill Climb (PPIHC) race and testing in 2017, along with supplier datasheet information. The thermal models developed predict the heat generation and temperatures of key components based on the current and power demand imposed to the components from lap time simulations. The completed model was utilized as a design tool to conduct thermal analysis of different powertrain configurations to create an optimized cooling system.

Acknowledgements

I would like to thank Dr. Marcello Canova for advising me for this research thesis. His knowledge on modeling of dynamic systems and the necessary steps for calibrating and verifying a model was essential in understanding the limitations and abilities for the thermal model of Buckeye Current's powertrain.

I would also like to thank Dr. Matilde D'Arpino for assisting me with the development of the models for the individual powertrain components and helping ensure the models reflected the physics of the electric machine and motor controller.

Finally, I would like to thank the Buckeye Current team and Center for Automotive Research for providing the opportunity to learn about electrified vehicles along with the necessary resources for me to develop as an engineer.

Table of Contents

List of Figures

List of Tables

Chapter 1: Introduction

Electrification in the Automotive Industry

Battery Electric Vehicles (BEV) provide an alternative to traditional internal combustion engines (ICE) and have potential to significantly reduce global emissions. The fuel economy for a BEV depends on the method of generating electricity in the country its operated in. Electricity generated through renewable energy has the largest environmental benefits, while coal power plants have minimal improvements compared to ICEs. Furthermore, the environmental impact of the collection and transportation of raw materials, inefficiencies in the infrastructure, and production of the vehicle must be considered [1]. A summary of the required miles per gallon (MPG) for an ICE vehicle to have the equivalent global emissions as a BEV for the five largest economies is shown in Table 1.

Table 1: Required fuel economy for ICE vehicle to have equivalent global emissions to average BEV by country [1]

Country	MPG
United States	55.4
China	40.0
Japan	44.3
Germany	52.1
United Kingdom	67.8

The effect of electricity generation method for the various countries is made clear from this table. Countries that produce a larger portion of their electricity from primary energy sources rather than fossil fuels, require ICE vehicles to have unattainable fuel economy to have equivalent emissions to a BEV. However, in countries were the electricity is generated from

non-renewables, such as China with many coal power plants, the emissions from a BEV are closer to those of an ICE vehicle. The fuel economies of most ICE vehicles are between 20 to 30 MPG [2], so despite the method of electricity production, BEVs provide benefits for all the major economies listed.

Despite dramatic advantages in fuel economy, adaptation of electrified vehicles has been slow. Some of the key predictors for an individual to purchase an EV are being environmentally conscious and a social innovator [3]. These are individuals which are influenced by climate change to pay more for an EV than a conventional ICE vehicle, and those who view EVs as a status symbol. However, as these technologies advance, consumer interests have expanded beyond environmental concerns to the performance of EVs [4]. By demonstrating the technological superiority of these vehicles, mainstream adoption of the new technology can be accelerated.

One method of showcasing advancement in electrified vehicle technologies is through zero emission racing, where electrified vehicles compete on the same courses as ICE vehicles. One of the largest motorsports, Formula One, now has an electric class, Formula E [4]. In this class, EVs compete on the same road circuits as Formula One, which has millions of viewers. The largest motorcycle road race in the world, the Isle of Man, has also introduced the TT Zero, which allows EV motorcycles to compete and be exposed to thousands of viewers on the island. By showcasing the performance capabilities of EVs through racing, adaptation can be accelerated in different demographics than just the environmentally conscious or social innovators.

Buckeye Current – Electric Racing at Ohio State

Buckeye Current is a student project team at the Center for Automotive Research at The Ohio State University. The team designs, builds, and races an all-electric motorcycle at professional competitions around the world. One of the main goals of the team is to help advance electric vehicle technology. Students who participate on the team learn valuable engineering, project management, and operation skills by working on detailed designs for the motorcycle. Buckeye Current also participates in various events to showcase the motorcycle and teach the public about electric vehicles, such as the student involvement fair, the American International Motorcycle (AIM) Expo, and visits with technical presentations for sponsors.

The team started in 2010 where they designed a motorcycle to set a land speed record with the East Coast Timing Association. Following this, the team had its debut with international racing competitions at the Isle of Man (IOM) TT Zero. The team had two 3rd place finishes at the IOM (2013, 2014) and then the team competed at Pikes Peak International Hill Climb (PPIHC) in Colorado, where they had one 2nd place finish (2015), one 3rd place finish (2016), and one 1st place finish (2017).

Electric racing requires the most advanced electric vehicle technology and helps identify opportunities for the greater electrified automotive industry. By participating in international competitions, developing talented engineers, and educating the public about electrified vehicles, Buckeye Current is helping in the effort to advance electrified vehicle technology and reduce CO2 emissions.

Design of Buckeye Current's Electrified Powertrain

Buckeye Current has competed at PPIHC for the past four years and is currently working on developing an all new motorcycle, RW-4, for the IOM in the summer of 2020. With the change in the race, one key feature that had to be reconsidered was the electrified powertrain. In an electric vehicle, the powertrain consists of an electric machine, a motor controller, a battery pack, and the overall vehicle controller. The interaction between these components for Buckeye Current's previous motorcycle, RW-3, is shown in Figure 1.

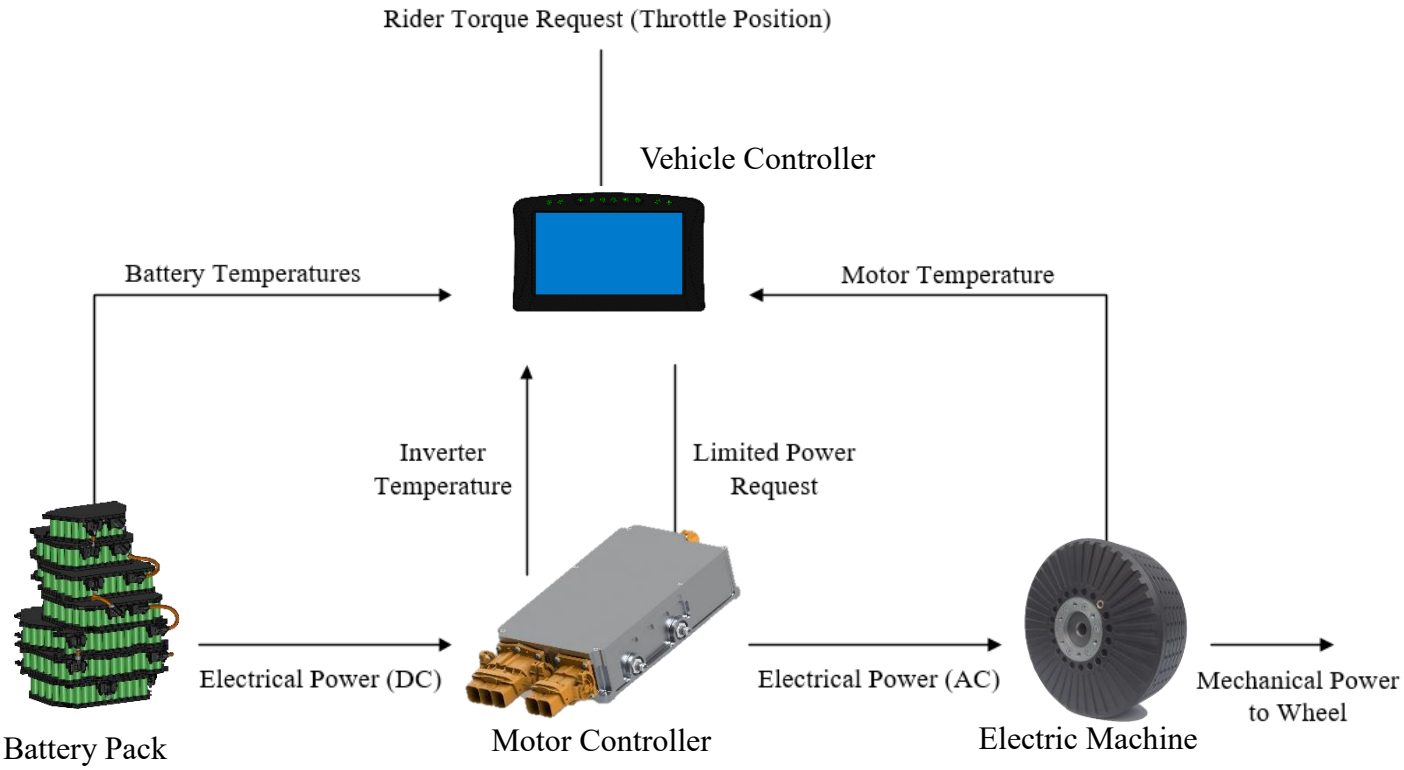

Figure 1: Electrified Powertrain for RW-3

Figure 1 illustrates how the rider's request for power is sent to the vehicle controller, which communicates with the motor controller. The motor controller then requests DC power from the battery pack and inverts this to AC electric power for the motor. During this operation, the temperatures of these major components are being reported to the vehicle controller to limit

power, if necessary, to prevent any of these components from being damaged by exceeding their maximum operating temperature.

The temperature of these components increases as their inefficiencies cause heat to be generated. The magnitude of heat energy depends on the operating conditions, power and current demand, of the component. For the electric machine and the motor controller, a water-based cooling system is required to dissipate the heat generated during racing. The cooling system that was used for RW-3 is shown in Figure 2.

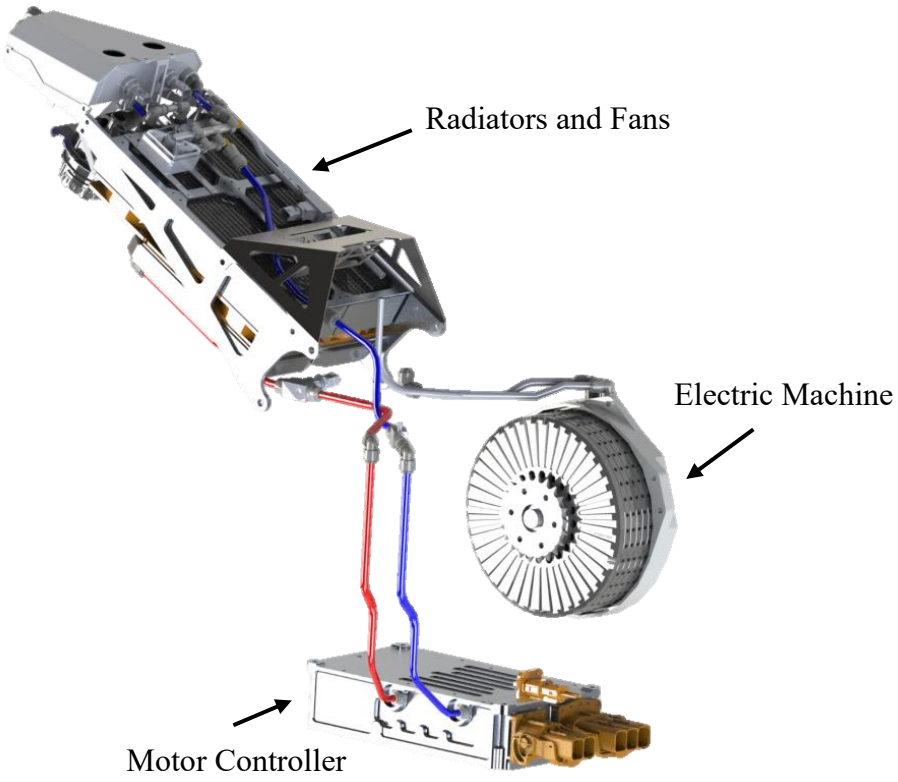

Figure 2: RW-3 Cooling System

This cooling system consisted of two separate cooling loops for the electric machine and motor controller. The reservoirs and pumps for the cooling system are integrated in the motorcycle's tail.

Research Objectives

The change from PPIHC to the IOM creates a new set of challenges for an electric powertrain. Pikes Peak is a 12.4-mile race, with 156 turns, and a 5,000 ft elevation change. This results in a powertrain that requires short periods of high-power demand. The Isle of Man is a 37.7-mile race, with long straightaways where gas-powered motorcycles exceed 200 mph. This requires long periods of high-power demand. These differences require an examination of the power output needed from the electrified powertrain and a consideration in the differences of the components' thermal performance.

This research focuses on designing an optimized cooling system for the RW-4 motorcycle. This requires developing physics based thermal models of the powertrain components, tuning these models using available data to reach strong agreement between the model prediction and measured data, then integrating these models with Buckeye Current's full vehicle simulation tools to predict the temperature rise of the powertrain components and determine cooling system requirements.

Chapter 2: Background

Overview of Thermal Modeling

Thermal modeling is the process of simplifying a physical system to simulate the transfer of heat within the system and estimate the temperature at different locations. One simplification method is known as lumped capacitance modeling [5]. This method assumes that the temperature within a mass is time varying but uniformly distributed throughout the solid. For this assumption to be valid, the heat conduction within a mass must be significantly greater than the heat transfer leaving the mass. This implies that the heat generated would distribute within the mass to a uniform temperature much faster than it would be dissipated to the environment. Biot's law is a criterion to determine if this modeling assumption is satisfied:

$$Bi = \frac{hL_c}{k} < 0.1, \quad L_c = \frac{V}{A_s} \tag{1}$$

where h is the heat transfer coefficient due to convection, k is the heat transfer coefficient due to conduction, L_c is the characteristic length, V is the volume of the solid, and A_s is the surface area of the solid.

The lumped capacitance modeling approach allows an extremely complex physical system to be approximated by a simpler thermal network. This greatly reduces computation time compared to methods that do not use such approximations, such as Finite Element Method (FEM), and allows the model to be integrated with larger vehicle simulations.

Previous Thermal Modeling Efforts

Thermal models of some of the individual powertrain components, the electric machine and radiator, have been proposed, which present a starting point for the development of the complete powertrain thermal model. However, thermal models of motor controllers were limited and a complete powertrain system thermal model for real time temperature predictions was not found.

Thermal analysis of electric machines can be conducted used FEM [6, 7] or using lumped parameter modeling with experimental data [8]. FEM gives the most accurate results, but it is computationally expensive; while lumped parameter models are computationally fast, but the accuracy of the results depends on the modeling assumptions and accuracy of the measured data.

Few thermal models have been created for motor controllers. The cooling system design for power electronics presented in [9] determined the requirements based on the heat generation in the IGBT module. However, this work did not develop a physics-based model of the component to evaluate different cooling system design options.

Radiators are complex components with many forms of heat transfer, but lumped parameter modeling techniques for them have been developed [10]. This process allows the radiator to be tuned with limited data available either from the supplier or measured.

Impact of this Research

Thermal modeling of a water-cooled electrified powertrain for cooling system design was not found. Therefore, to determine the cooling system requirements for Buckeye Current's electric motorcycle, thermal models of the electric machine, motor controller, and radiators must be adapted from literature and integrated to Buckeye Current's simulation tools to be used for a

design optimization. This requires simplifying previous thermal models based on available data and physics of the components.

In this research, an original single node motor controller thermal model is developed to accurately predict the key operating temperature while being computationally efficient. This research also develops a technique for determining unknown motor model parameters relying only on data provided by the motor supplier since no experimental data was available. Finally, this research demonstrates a process of integrating low order, accurate thermal models into vehicle simulation tools for cooling system design and evaluating powertrain thermal performance.

Chapter 3: Development of Physics Based Models

Methodology

Due to limitations in data available for the powertrain components and need to predict real-time component temperatures for cooling system design, the thermal models will use a lumped parameter modeling approach. To create thermal models of the components that accurately predict temperatures in the physical system using this method, the design and internal geometry of each component will be analyzed and considered. Then, the heat generation will be applied in the appropriate node of the thermal network that matches the physical system. Finally, the conservation of energy will be used to derive the equations the model and determine how heat is transferred through the system. Existing thermal models of powertrain components will be referenced when available to ensure the models match the physics of the component. Since the goal of this thermal system and the thermal models is to be integrated with a larger, full vehicle simulation, a fast-computational time is vital. Therefore, the degrees of freedom of each model will be reduced as much as possible while maintaining a high accuracy compared to measured data.

Motor Controller Thermal Model

To determine which portions of the motor controller were necessary in the thermal network of the component, the internal geometry of the motor controller and the operation of the component were considered. For a motor controller to operate an AC electric machine with a DC battery pack, the DC current must be inverted to AC current. This is performed with pulse width modulation, which is quickly switching DC current on and off using power electronics. The power electronics used in Buckeye Current's motor controller are IGBTs. There are three

IGBT modules as radial flux motors require three phases of AC current to operate, each IGBT module corresponds to a phase. This switching operation is the main source of losses in the motor controller and the small thermal mass of the modules causes the temperature to increase quickly.

As the IGBT modules are the main source of losses and heat generation in the motor controller, these three modules rest directly on top of the cooling block. The typical configuration of the power electronics resting on top of the cooling block is shown in Figures 3 and 4.

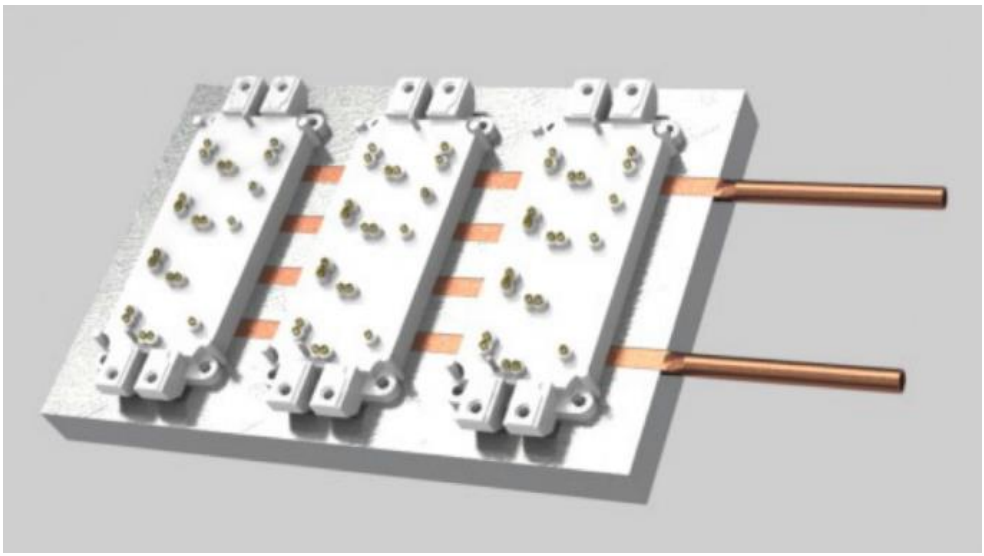

Figure 3: IGBT Modules on top of Cooling Block, isometric view [9]

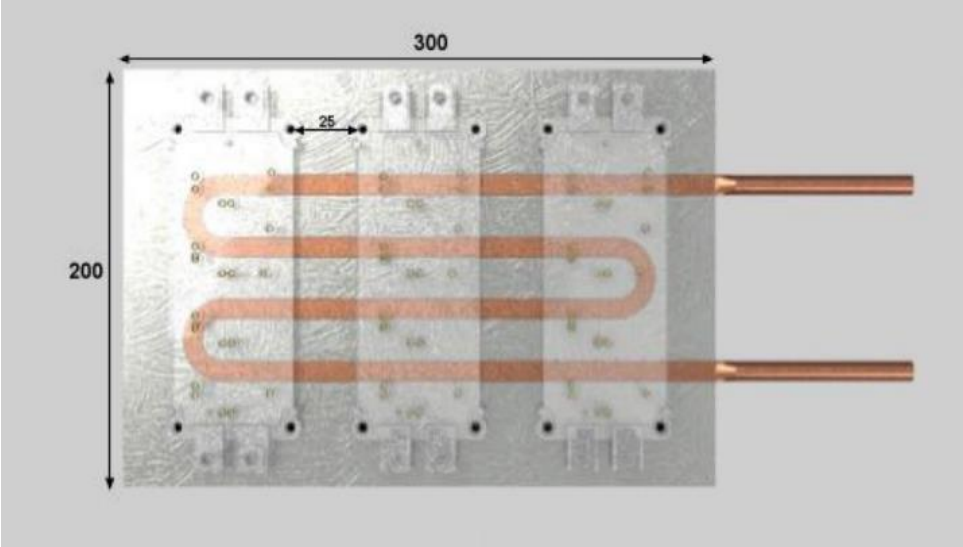

Figure 4: IGBT Modules on top of Cooling Block, top view [9]

From data collected by Buckeye Current, we can gain an understanding of the temperatures of key motor controller components while racing.

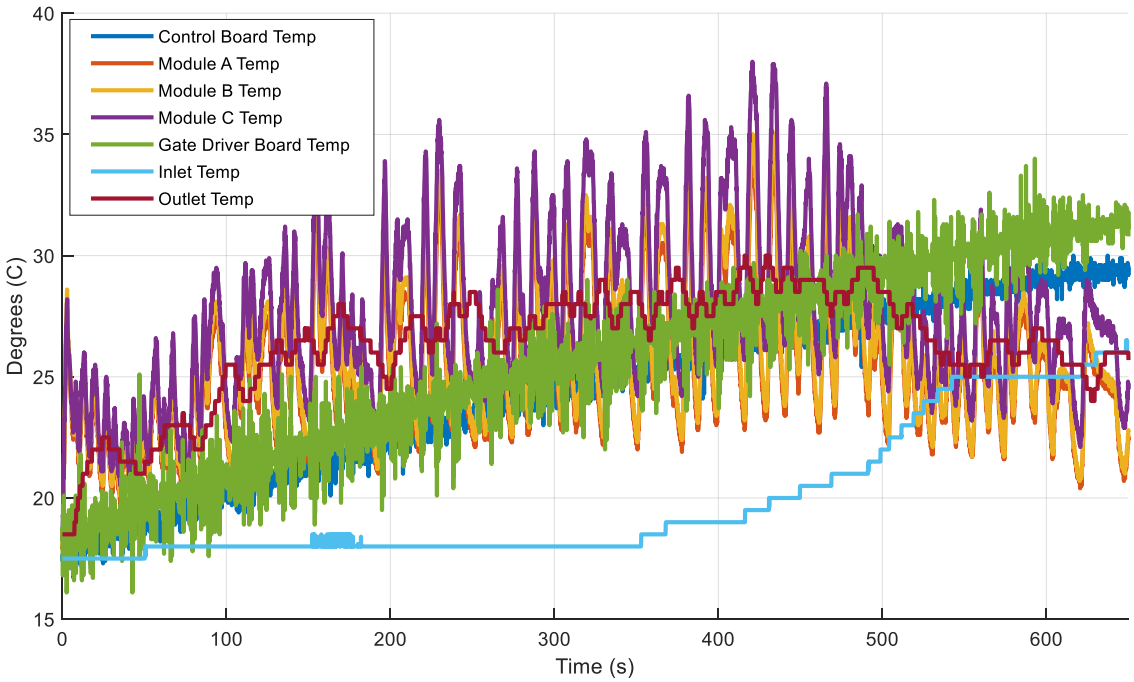

Figure 5: Motor Controller Measured Temperatures at PPIHC 2017

This data show that when the motorcycle is operating at full power levels, the power electronics in the switching modules are at the highest temperature. The motorcycle became power limited later in the race because the voltage of the battery pack dropped as the battery cells reached a low state-of-charge. When this happened, the control board and gate driver board temperatures exceeded the temperatures of the IGBT modules. This occured because these components are further from the cooling block and must reject heat through the IGBT modules. At low power levels, the heat rejection in the modules is low, which allows them to stay below the temperature they raised these other components to when the heat rejection was higher. This temperature dynamic is only present when the power output of the motor controller is greatly reduced, this is an unwanted feature as it will reduce motorcycle performance. RW-4 will be designed to prevent this behavior.

If any of the components within the motor controller approach the maximum operating temperature, the power must be limited to prevent overheating. Since the IGBT modules are at the highest temperature during normal operation, these are the critical components that the thermal model of the motor controller must predict. Further, Figure 5 shows that the temperatures of the three modules are very similar, so to reduce complexity in the model, it is assumed that all modules operate at the average temperature. Based on these assumptions, a single node thermal model of the motor controller can be created.

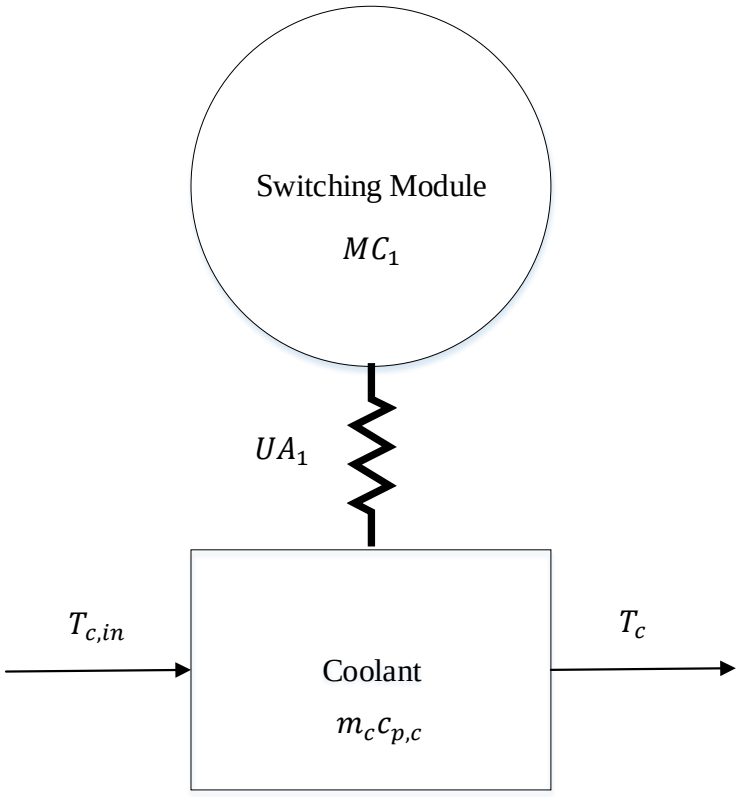

Figure 6: Motor Controller Thermal Model (MCTM)

The thermal model of the motor controller lumps the three switching modules into a single thermal mass. This thermal model is described by the following set of equations:

$$MC_1 \frac{dT_1}{dt} = \dot{Q}_{heat} - UA_1(T_1 - T_{c,in})$$
$$m_c c_{p,c} \frac{dT_c}{dt} = \dot{m}_c c_{p,c}(T_{c,in} - T_c) + UA_1(T_1 - T_{c,in}) \quad (2)$$

where MC_1 is the heat capacitance of the IGBT module, $\dot{Q}_{heat}$ is the heat generated, T_1 is the temperature of the inverter module, $T_{c,in}$ is the inlet coolant temperature, UA_1 is a lumped heat transfer coefficient representing all forms of heat transfer between the power electronics and the coolant, $m_c c_{p,c}$ is the heat capacity of the coolant where $c_{p,c}$ is the specific heat of water, this term is required because the time constant for the coolant differs from the IGBT modules, T_c is the outlet coolant temperature, and $\dot{m}_c$ is the coolant mass flow rate.

The inputs for this model are the RMS electric machine current and the battery pack DC bus voltage to estimate the losses of the motor controller, the inlet temperature of the coolant, and the mass flow rate of the coolant. Then the outputs of the model are the temperature of the lumped switching module and the outlet coolant temperature. These are summarized in the following figure:

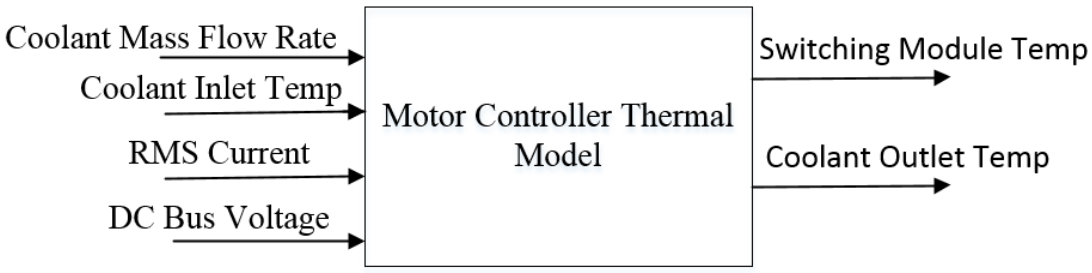

Figure 7: MCTM Inputs and Outputs

Electric Machine Thermal Model

An electric machine creates mechanical energy from electrical energy. There are many designs available, however one common machine for high power density application such as racing is a permanent magnet synchronous machine (PMSM). This machine consists of a rotor containing permanent magnets, stator winding, and a stator core. For a PMSM, the magnetic field that is generated by the electricity to produce mechanical energy can be applied either axially or radially with respect to the permanent magnets. Based on a review of the two technologies and lap time simulations, the Buckeye Current team has decided to use a radial flux motor for the IOM. The internal layout of this type of machine is shown in Figures 8 and 9.

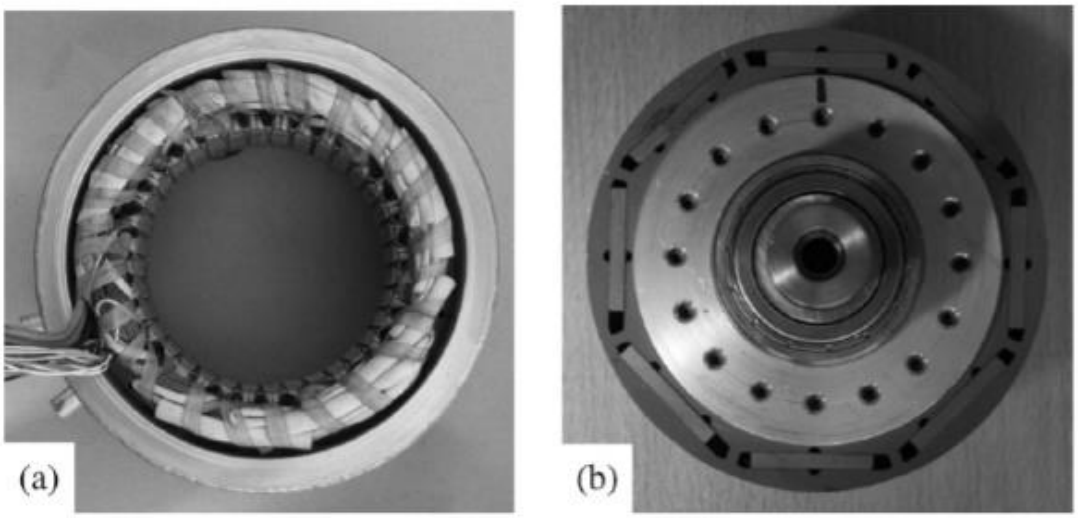

Figure 8: Internal PMSM (a) Stator and (b) Rotor [8]

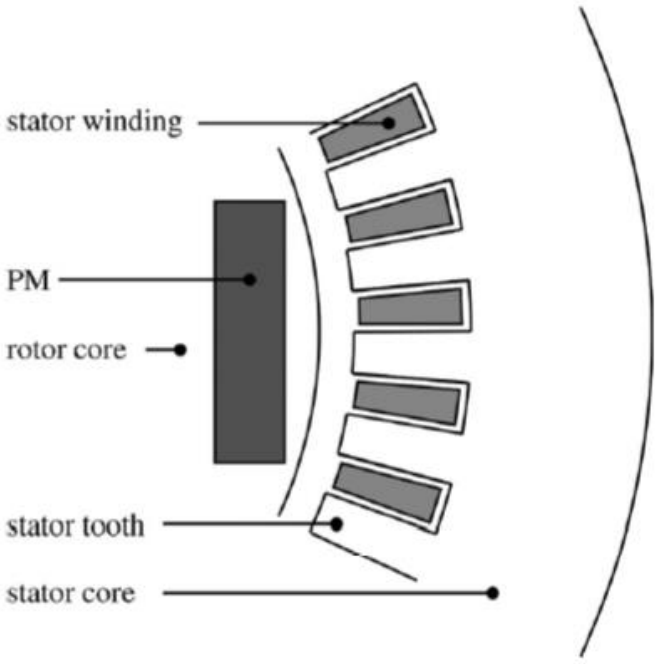

Figure 9: Diagram of Internal PMSM structure [8]

From the internal geometry of the machine, a physics based thermal model was presented in [8]. The radial flux motor thermal model is shown in Figure 10.

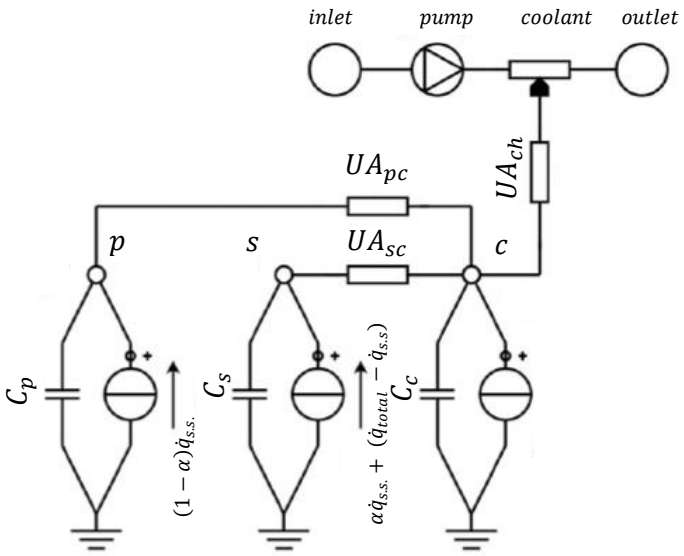

Figure 10: Simplified thermal model with three nodes: permanent magnets *p*, stator winding *s*, and stator core *c* [8]

This thermal model captures the three main motor components: the permanent magnets, the stator winding, and the stator core. C_p represents the heat capacity of the rotor, T_p is the temperature of the rotor, and P_p is the power dissipated in the rotor. $C_s, T_s,$ and P_s are the same terms for the stator winding and $C_c, T_c,$ and P_c are the terms for the stator core. G_{pc} is the lumped thermal resistance, representing convection, conduction, and radiation, between the rotor and the stator core. G_{sc} is the lumped thermal resistance between the stator windings and the stator core, and G_{ch} is the lumped thermal resistance between the stator core and the coolant. To avoid an algebraic equation in the thermal model, P_c was assumed to be negligible. This thermal model is described by the following set of equations:

$$C_p \frac{dT_p}{dt} = (1-\alpha)\dot{q}_{s.s.} - UA_{pc}(T_p - T_c)$$

$$C_s \frac{dT_s}{dt} = \alpha\dot{q}_{s.s} - UA_{sc}(T_s - T_c) + (\dot{q}_{total} - \dot{q}_{s.s}) \quad (3)$$

$$C_c \frac{dT_c}{dt} = UA_{pc}(T_p - T_c) + UA_{sc}(T_s - T_c) - UA_{ch}(T_c - T_{cool,\,in})$$

$$m_{cool}c_{p,cool} \frac{dT_{cool}}{dt} = \dot{m}c_{p,cool}(T_{cool,\,in} - T_{cool}) + UA_{ch}(T_c - T_{cool,\,in})$$

where $\dot{q}_{total}$ is the total heat rejection of the electric machine, $\dot{q}_{s.s}$ is the heat rejection of the electric machine at the continuous power level at the operating RPM, UA_{pc} is the inverse of G_{pc}, UA_{sc} is the inverse of G_{sc}, UA_{ch} is the inverse of G_{ch}, α is the portion of heat rejected in the winding, $m_{cool}c_{p,cool}$ is the heat capacity of the coolant, $\dot{m}$ is the coolant mass flow rate, $c_{p,cool}$ is the specific heat of water, $T_{cool,\,in}$ is the inlet coolant temperature, and T_{cool} is the outlet coolant temperature. The inclusion of $\dot{q}_{total}$ and $\dot{q}_{s.s}$ is necessary as the additional heat rejected from increasing motor torque at a given RPM is from additional losses in the stator winding from the increased phase currents, so the distribution of heat from α is only for the continuous power specification.

The inputs to this model are the heat distribution, alpha, the coolant mass flow rate, the coolant inlet temperature, the total heat rejection and the continuous power heat rejection. The outputs are the stator winding, stator core, rotor, and coolant outlet temperatures.

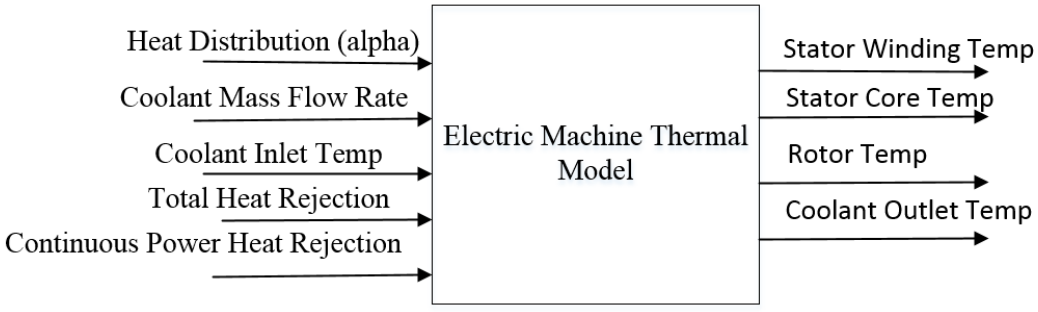

Figure 11: EMTM Inputs and Outputs

Radiator Thermal Model

Radiators are complex systems and much of the data needed for creating a thermal model is proprietary. However, the method of developing physics based thermal models was described in [10] and consists of breaking the radiators into a series of thermal nodes consisting of the coolant, the metal tubes and fins, and the air.

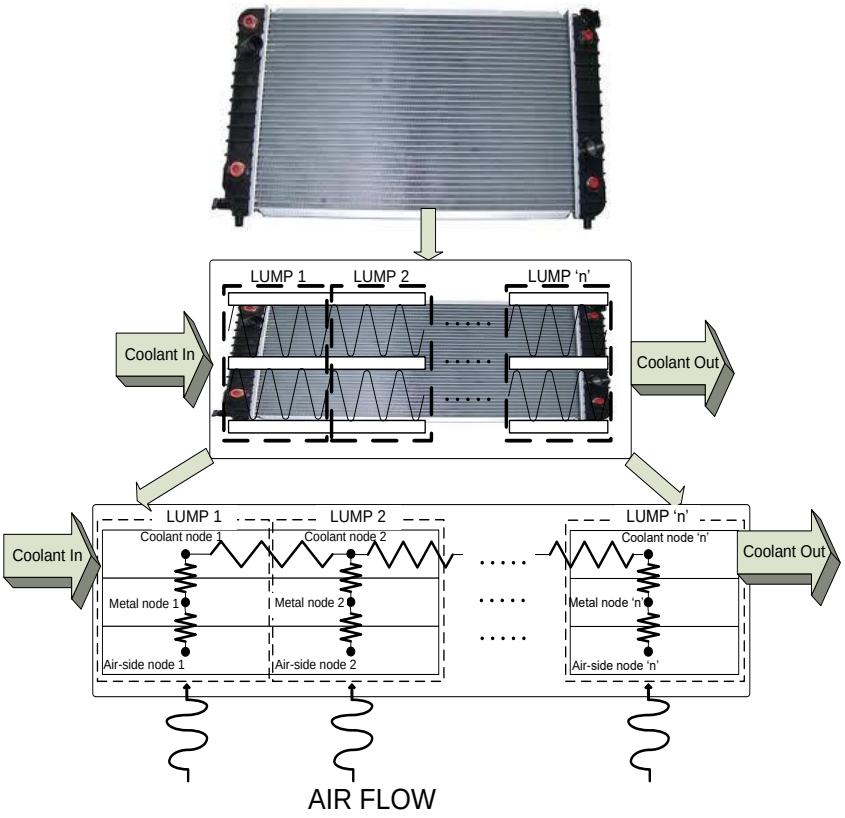

Figure 12: Radiator Thermal Modeling Process [11]

The equations describing this thermal model have been previously developed at the Center for Automotive Research. Each thermal node has the same behavior but with different input conditions, so by assuming a single node the order of the model can be greatly reduced while maintaining accuracy [11]. This results in the following equations to describe the radiator model:

$$C_c \frac{dT_c}{dt} = \dot{m}_c c_{p,c}(T_{c,in} - T_c) - A_f * \frac{C_f \dot{m}_c^{\beta}}{C_3}(T_c - T_w)$$

$$C_w \frac{dT_w}{dt} = A_f * \frac{C_f \dot{m}_c^{\beta}}{C_3}(T_c - T_w) - A_f \frac{1}{C_2}(T_w - T_s) \quad (4)$$

$$C_s \frac{dT_s}{dt} = A_f \frac{1}{C_2}(T_w - T_s) - A_f \frac{(\rho_{air} V_{face})^{\frac{2}{3}}}{C_1}(T_s - T_{air})$$

where C_c, C_w, C_s are the thermal masses for the coolant, walls of the radiator, and fins of the radiator, T_c, T_w, T_s are their corresponding temperatures, C_1, C_2, C_3 are tuning parameters used to calibrate the heat transfer coefficients and are determined experimentally, A_f is the area of the radiator face, V_{face} is the velocity of air at the radiator face, ρ_{air}, T_{air} are the density and temperature of the ambient air, $\dot{m}_c$ is the mass flow rate of the coolant, and C_f is capacity of the fluid, and β is the slope of the saturated air enthalpy vs. temperature line.

The inputs to this model are the air temperature, face velocity, air density, coolant mass flow rate, and coolant inlet temperature. Then the outputs are the coolant outlet temperature, the wall temperature, and the fins temperature.

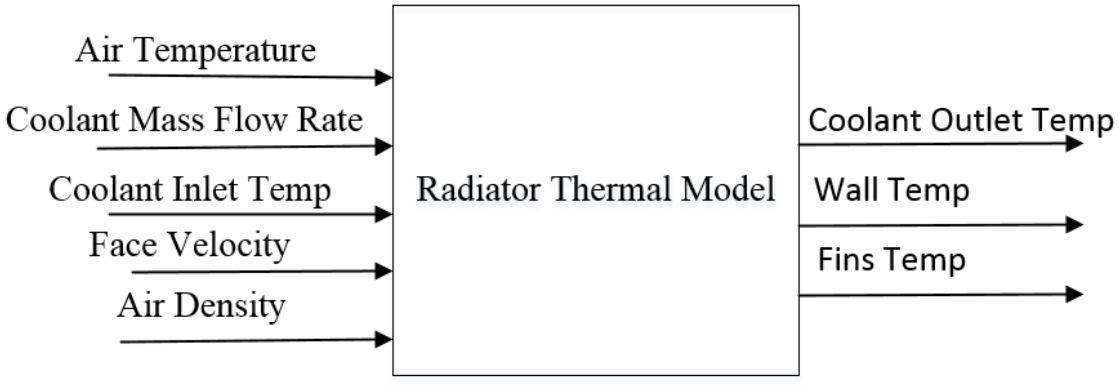

Figure 13: Radiator Thermal Model Inputs and Outputs

Reservoir Thermal Model and Pump Considerations

The coolant reservoir is important to introduce an additional thermal mass to reduce temperature fluctuations of the coolant. The coolant reservoir can be modeled as a single thermal mass with the only forms of heat transfer being coolant entering and leaving the reservoir. It is assumed that radiation with the surroundings and conduction is negligible due to the small temperature difference and high thermal resistance. These assumptions result in the following equation for the reservoir:

$$m_c c_{p,c} \frac{dT_c}{dt} = \dot{m}_c c_{p,c}(T_{c,in} - T_c) \tag{5}$$

where T_c is the temperature of coolant in the reservoir, m_c is the mass of coolant in the reservoir, $c_{p,c}$ is the specific heat of water, $\dot{m}_c$ is the mass flow rate, and $T_{c,in}$ is the inlet coolant temperature.

Besides acting as a damper to the coolant temperature, the reservoir is also important to provide sufficient pressure to prevent cavitation in the pump. Cavitation can occur when the fluid reaches its saturation pressure in the pump. This can lead to inconsistent flow and cause damage to the pump. The quantity used to determine if there is adequate pressure to avoid saturation is the net positive suction head (NPSH). The NPSH available at the pump is defined by the difference between the pressure at the pump inlet and the saturation pressure of the fluid:

$$NPSH = \frac{p_{inlet}}{\rho g} - \frac{p_v}{\rho g} \tag{6}$$

where p_{inlet} is the inlet pressure of the pump, p_v is the saturation pressure of the coolant, ρ is the density of the fluid, and g is gravity. The required NPSH is generally provided by the pump manufacturer.

To choose an appropriate pump for the application, the pressure drops in the system along with the required flow rate must be determined. For Buckeye Current's powertrain, the approximate pressure drops for the electric machine, motor controller, radiator, flow rate sensor, and tubing at 10 liters per minute flow rate and 60 C coolant temperature, 50/50 water and glycol mixture, are summarized in Table 2.

Table 2: Pressure Drops in RW-4 Cooling System

Component	**Pressure Drop [bars]**
Electric Machine (Parker GVM 210-100)	0.2
Motor Controller (Rinehart PM150DZ)	0.35
Radiator (Yamaha R1 Radiator)	Unknown
Flow Rate Sensor (Omega FTB2006)	0.138
Tubing (Nylon braided rubber tube)	0.05

Since the pressure drop in the radiator is unknown, it must be determined experimentally during the assembly of the cooling system. However, if the pressure drop is like the other components in the system, then the pump must be able to deliver approximately 0.95 bars of pressure if the coolant flow rate is 10 LPM.

Chapter 4: Calibration of Parameters of Thermal Models

Motor Controller Calibration

The same model motor controller that will be used for RW-4, the Rinehart PM150DZR, was also used by the Buckeye Current team in the 2017 and 2018 race seasons. In 2018, the coolant outlet temperature sensor wasn't operating properly, so the data from 2017 was used to tune the parameters of the thermal model. Data collected during testing prior to the race was used to calibrate the model and then the PPIHC 2017 race data was used to determine how accurately the calibrated model predicted the module temperatures.

The four datasets used to calibrate the motor controller thermal model are shown in Figure 14.

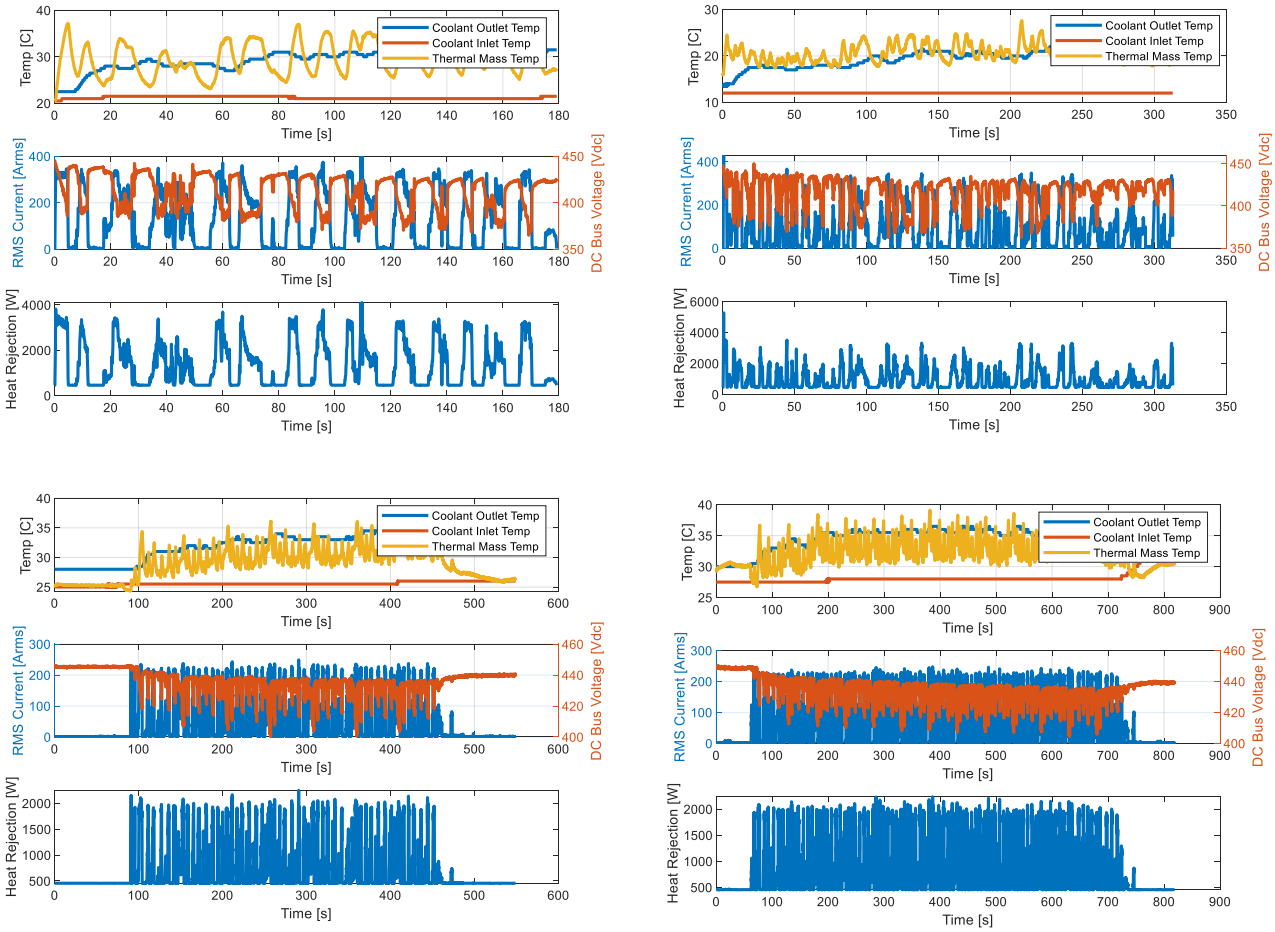

Figure 14: Tuning Data for MCTM

This data contains the average temperature of the switching modules, the inlet and outlet coolant temperatures, the RMS current, and the DC bus voltage. The RMS current was calculated based on the following:

$$I_{rms} = \sqrt{I_q^2 + I_d^2} \tag{7}$$

where I_q is the torque producing current the motor controller sends to the electric machine and I_d is the portion of the current that resists the back-emf generated by the motor. These currents

were measured by the motor controller. Using the RMS current and the bus voltage, the losses in the motor controller can be estimated from an equation provided by the manufacturer:

$$P_{loss} = 0.000244 * V_{DC}^{1.072} * I_{RMS}^{1.695} + 456.4 \quad (8)$$

where P_{loss} is the power loss in Watts, V_{DC} is the DC bus voltage, and I_{rms} is the RMS current.

The non-operating portions of the data in (c) and (d) were eliminated and the data were combined into a single dataset. The discontinuities between the datasets are small relative to the rest of the data, so the error these will produce can be ignored. This combined dataset is shown in Figure 15.

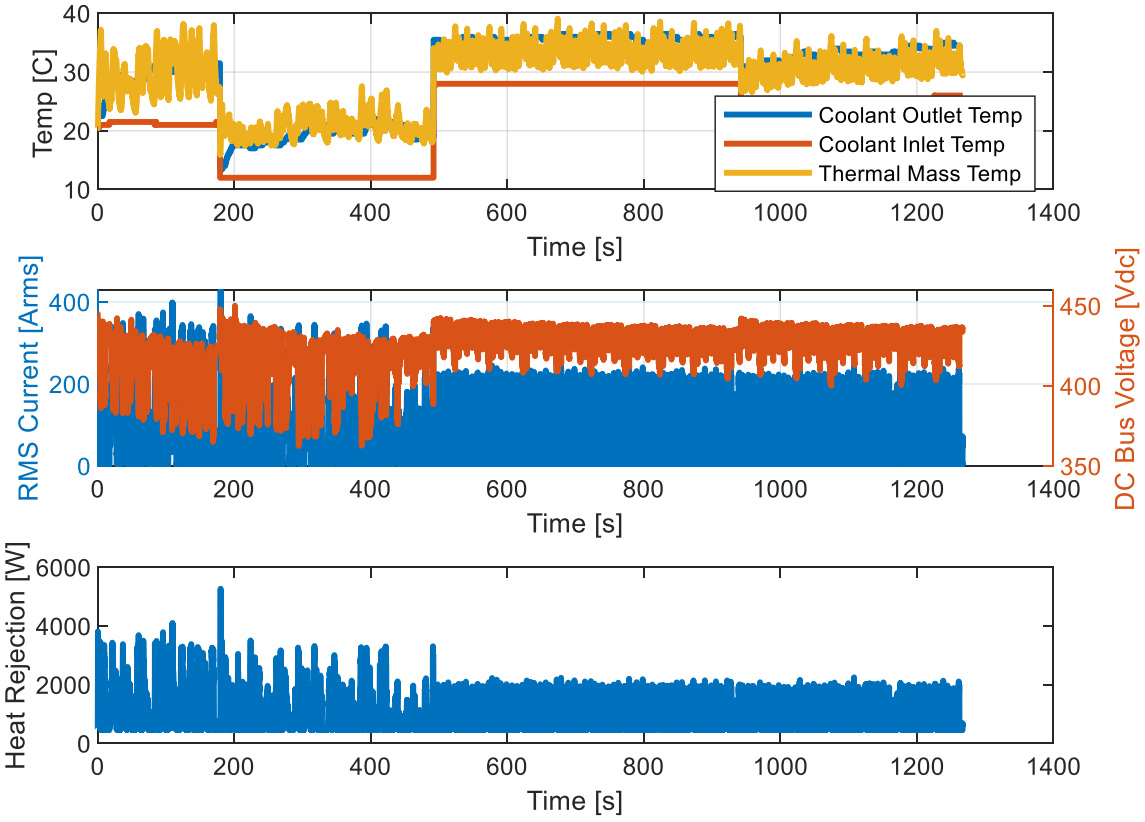

Figure 15: Combined Data for Inverter Thermal Model

This dataset will be used to calibrate the parameters in the motor controller thermal model. The tuning method will be using an unconstrained nonlinear optimization method in MATLAB, *fminsearch.m*. To use this algorithm, initial guesses must be made for the unknowns and an objective function must be specified. For this model, the objective function was the minimization of the least square error between the model and the data for both the thermal mass temperature and the coolant outlet temperature, and the unknowns in the thermal model were estimated based on the physical properties of the motor controller. These unknowns are summarized in Table 3.

Table 3: Initial Estimates of Unknown Parameters for Motor Controller

Parameter	**Initial Guess**
MC_1	500 J/K
UA_1	100 W/K
$\dot{m}_c$	8 L/min
m_c	0.0545 kg

The heat capacitance of the motor controller, MC_1, was estimated based on the specific heat of aluminum and the mass of the module and cooling block. The overall heat transfer coefficient, UA_1, was a guess based on reasonable values of conduction and convection. The flow rate of coolant, $\dot{m}_c$, was assumed to be equal to the recommended flow rate from the manufacturer since flow rate data was unavailable, and the mass of coolant in the system, m_c, was estimated based on the volume of the cooling channels and tubing between the inlet and outlet temperature sensors and the density of water.

To use *fminsearch.m* to identify the model parameters, the model must be defined in a mathematical format for optimization. To have a model which accurately predicts the temperature, the error between the model and the data must be minimized. The temperature of the switching module and the outlet coolant temperature are both important for the model to accurately predict, so the optimization minimizes the sum squared error of both:

$$f\colon\ \varepsilon_{T1} + \varepsilon_{T2} \tag{9}$$

where,

$$\varepsilon_{T1} = \sum \frac{(T_{1,model} - T_{1,data})^2}{N} \tag{10}$$

$$\varepsilon_{T2} = \sum \frac{\left(T_{2,model} - T_{2,data}\right)^2}{N} \tag{11}$$

where T_1 is the switching module temperature, T_2 is the coolant outlet temperature, and N is the number of samples.

The optimization algorithm then iteratively searches through possible numerical values of the parameters, π, until the error function reaches a minimum:

$$\pi^* = min\ f(x, \pi, t) \tag{12}$$

where f is the error function defined in equation 9, π^* are the set of parameters with their optimized values, x are constants for the model, π is the set of parameters which can be optimized, for the motor controller $\pi = \{MC_1, UA_1, \dot{m}_c, m_c\}$, and t is time.

The predicted motor controller temperature compared with the combined test data is shown in Figure 16 along with the error correlation plots in Figures 17 and 18.

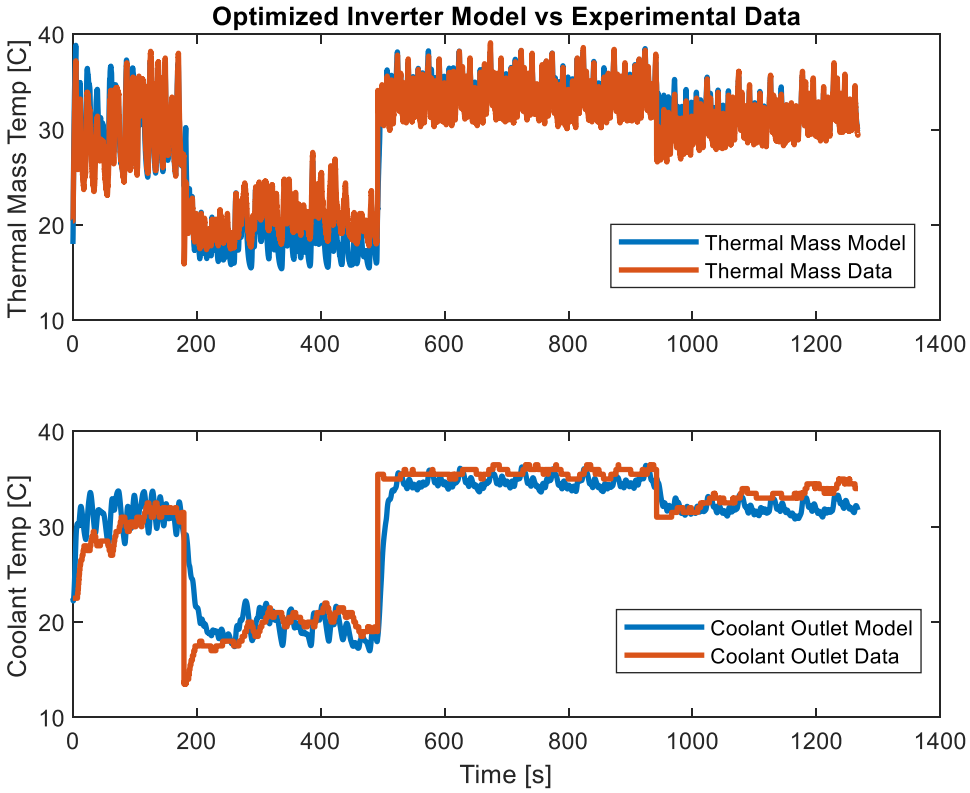

Figure 16: Optimized MCTM

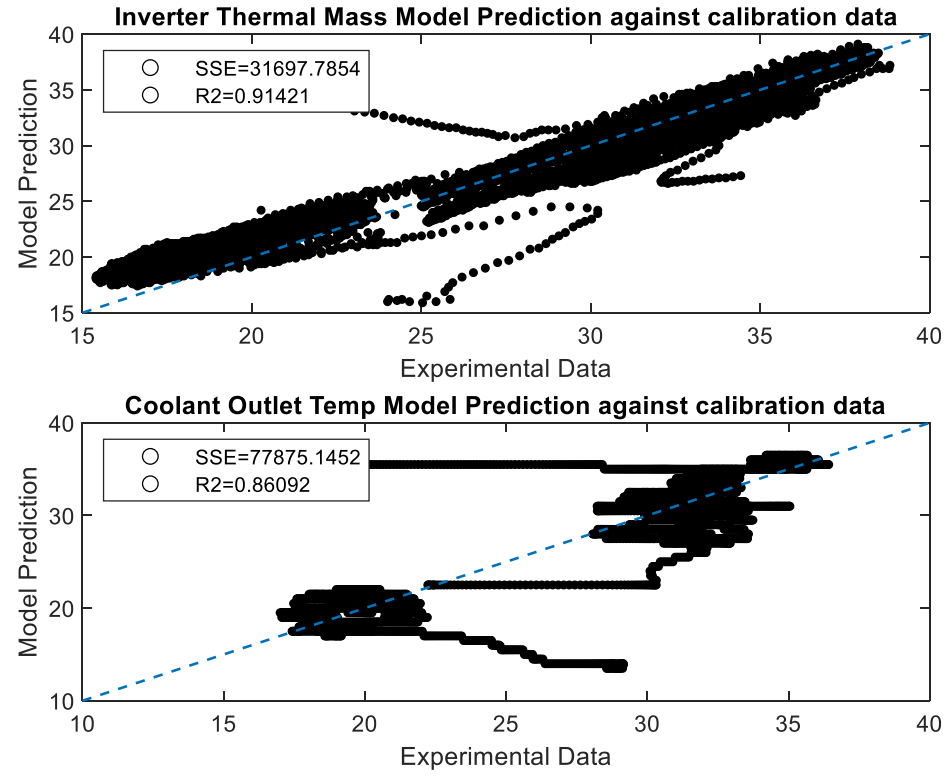

Figure 17: MCTM Error Correlation Plot

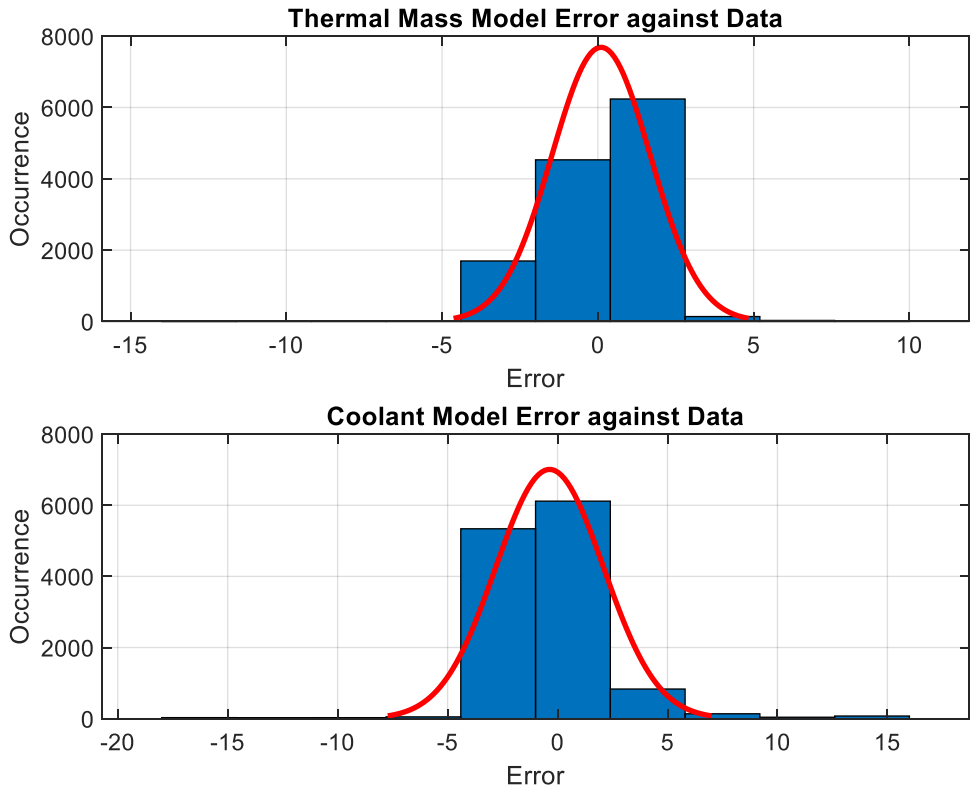

Figure 18: Motor Controller Error Distribution Plot

From Figure 16, we can see that the predicted temperatures from the model are very close to the data. This is confirmed from Figure 17, where the R^2 values for both the thermal mass temperature and the coolant outlet temperature are strong, especially considering the discontinuities in the combined dataset. Finally, Figure 18 shows small values for the error for both the thermal mass and the coolant outlet temperature. The thermal mass has a biased error distribution, but the small magnitude of the error makes this model acceptable.

The final analysis of the tuned model consists of determining if the calibrated parameters are reasonable physical values and testing the model against data that wasn't used in the calibration process. The tuned parameters from the optimization algorithm are shown in Table 4.

Table 4: Tuned Parameters of Motor Controller Thermal Model

Parameter	Initial Guess
MC_1	363.2 J/K
UA_1	143.9 W/K
$\dot{m}_c$	1.875 L/min
m_c	0.1995 kg

The changes are small from the initial guesses, which were based on the physical system, for all parameters except the coolant flow rate. This change is reasonable however, as the coolant flow rate in the actual bike was unknown and is possible that it was much lower than the recommended flow rate.

Race data from PPIHC 2017 was used to compare the tuned thermal model to data not used in the calibration process. At PPIHC in 2017, the battery pack dropped to a low SOC towards the end of the race which made the motorcycle power limited. Since reaching the temperature limit in power limited situation is unlikely, this portion of the data was discarded for the comparison. This data set is shown in Figure 19.

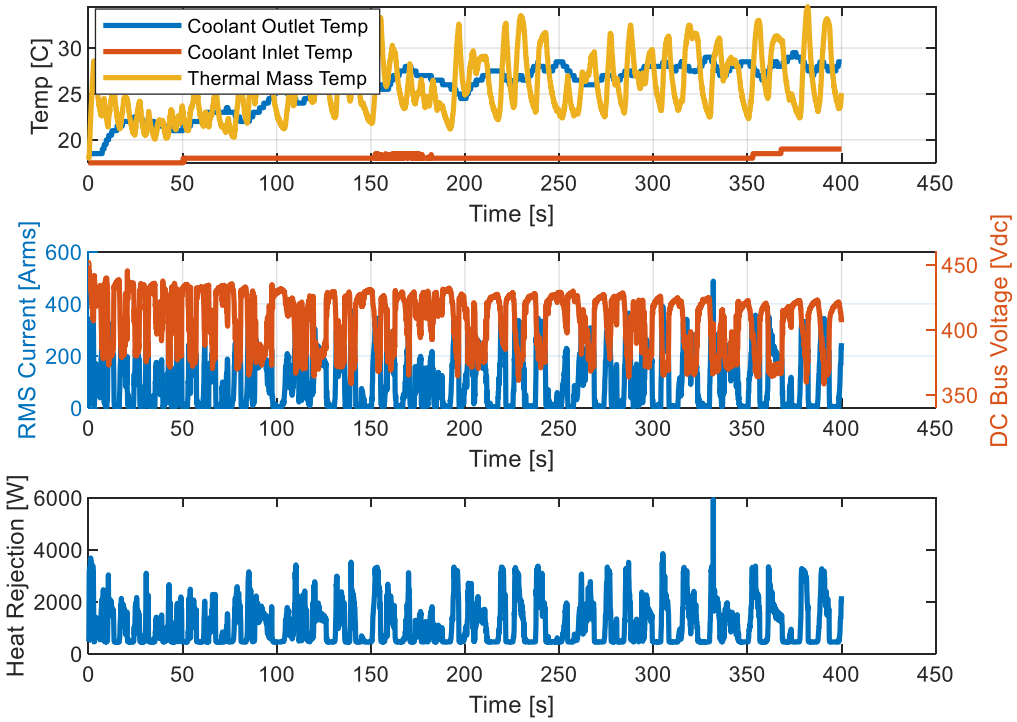

Figure 19: PPIHC 2017 Data used for Model Analysis

This dataset contains all the required data for the thermal model to predict the temperature. The parameters found by the optimization algorithm and listed in Table 3 were used to predict the temperature of the motor controller under this power demand. The results are shown in Figure 20 and the error correlation plots are shown in Figure 21 and 22.

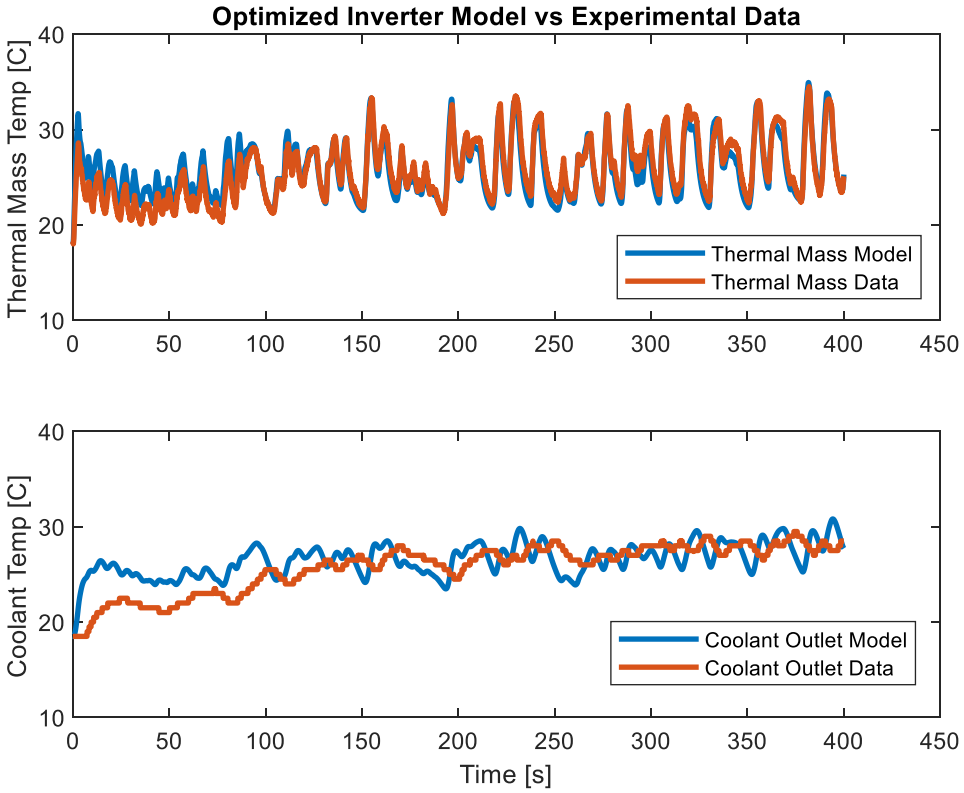

Figure 20: Model Prediction Versus Measured Data

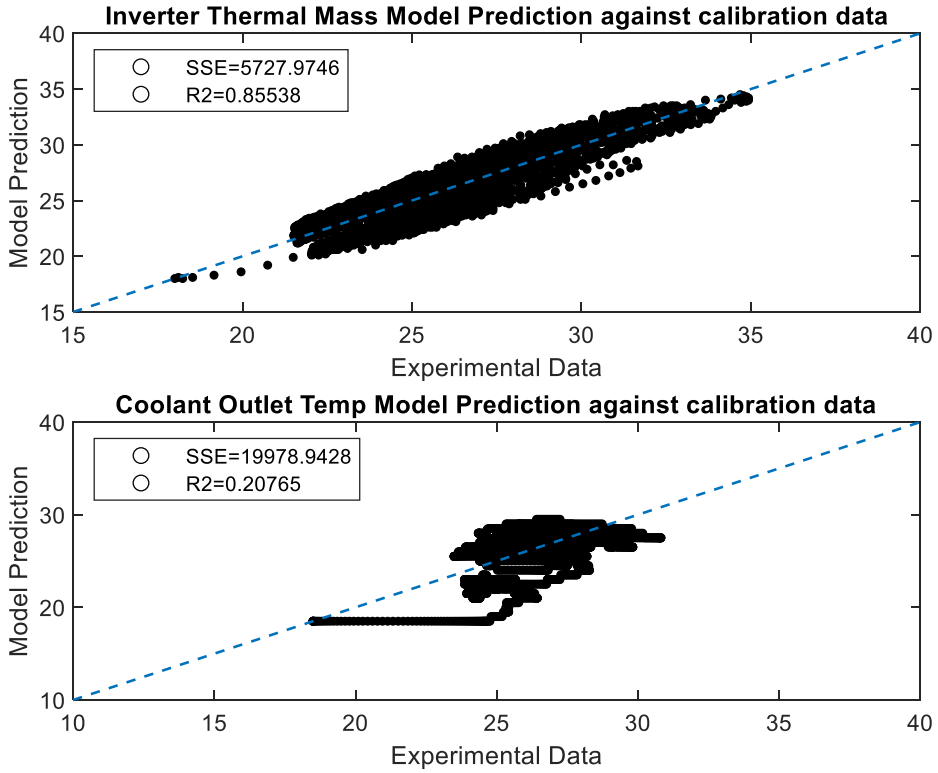

Figure 21: Non-Calibrated Dataset MCTM Error Correlation

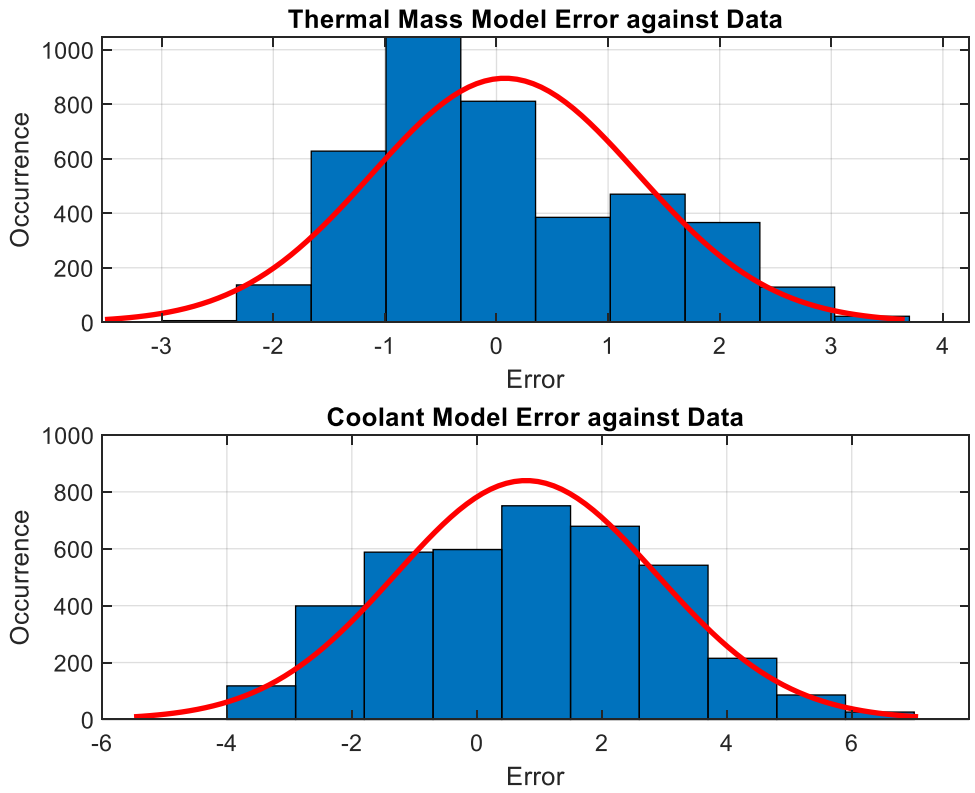

Figure 22: MCTM Error Distribution Plot

These figures confirm that the thermal model is predicting the temperatures of the motor controller accurately. Figure 20 shows the thermal mass is being predicted very accurately and the coolant outlet temperature is initially different from the collected data, but this is likely due to the slow time constant of the coolant outlet temperature sensor. Figure 21 shows a strong R^2 value for the thermal mass, but the errors introduced by the temperature sensor measurement lead to a small R^2 value for the coolant outlet temperature. Finally, Figure 22 shows the error between the model and the measured data is small and normally distributed.

Based on the analysis of the tuned parameters values, the error correlation plots, and the predicted temperatures from the thermal model, this single node motor controller thermal model is very accurate with a fast computation time. The complete motor controller thermal model with all its parameters is summarized in Appendix A.

Electric Machine Calibration

For the entire history of the team, Buckeye Current has used axial flux motors rather than radial flux motors. The internal geometry between these two machines is different and they require different thermal models as the heat transfer within the machines is different. The motor chosen for the IOM in 2020 is a radial flux motor, so the thermal data previously collected by the team is not valid for calibration of the motor thermal model. Also, the motor has been ordered but has not arrived, so no thermal data from testing is available. Therefore, only data provided by the electric machine manufacture datasheet is available to determine the parameters of the motor thermal model.

All electric machines have a peak power rating and a continuous power rating. Peak power is the maximum amount of torque that can be produced by the machine at any given rotational speed, while continuous power is the torque the machine can produce at any given rotation speed without overheating if the cooling conditions match those specified in the datasheet. For the Parker GVM 210-100 motor with 50/50 water/glycol coolant at 60C inlet temperature, the continuous and peak power torque-speed curves are shown in Figure 23. Parker also provided the losses of the motor at any given torque-speed operating point. The losses of the machine at the continuous power operating points are shown in Figure 24.

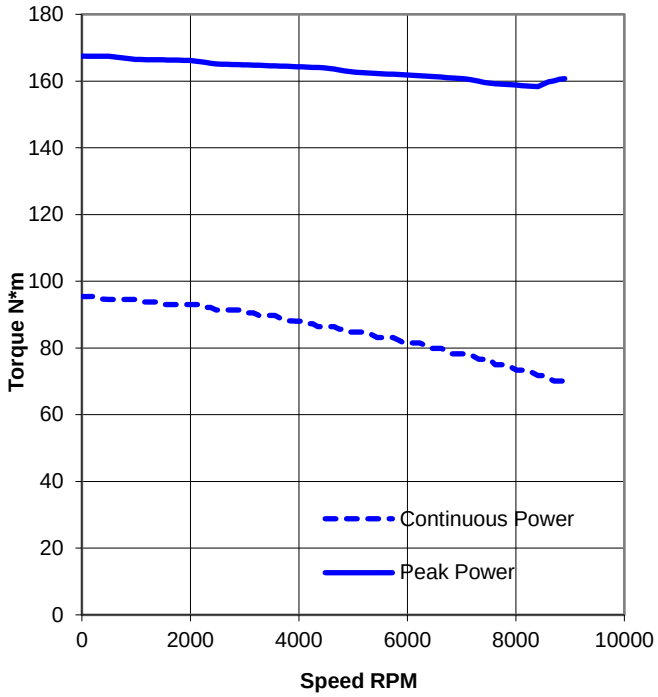

Figure 23: Torque Speed Curve for Parker GVM 210-100 J6 Winding [12]

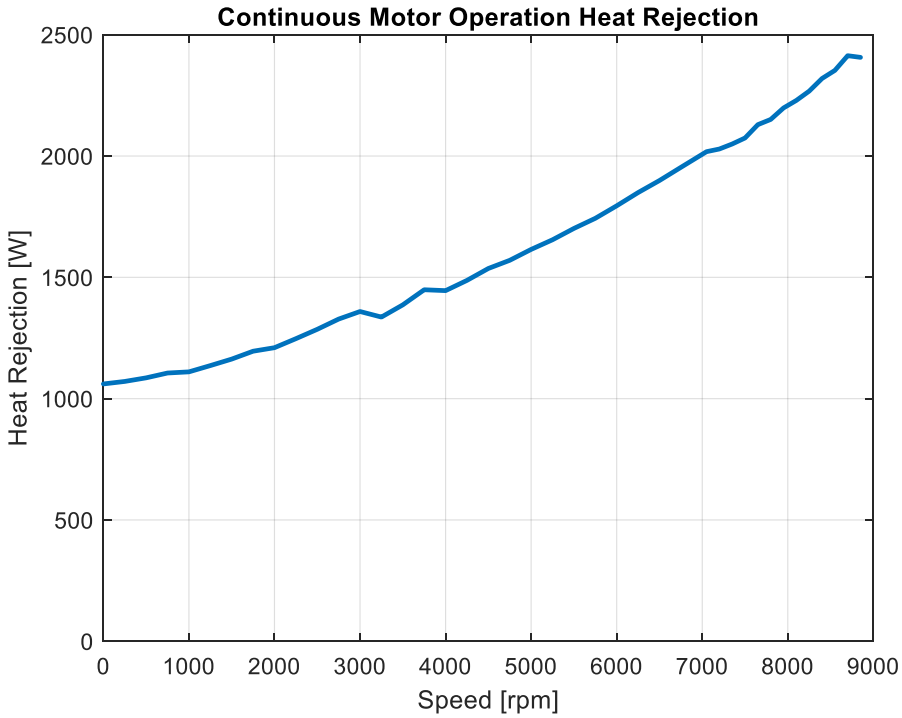

Figure 24: Electric Machine Continuous Power Heat Rejection

The continuous power curve provides a series of steady state operating points for the electric machine. Therefore, these points can be used to tune the unknown parameters in the motor thermal model if the equations describing the model are simplified to steady state equations. The simplified equations are:

$$\begin{aligned} 0 &= (1-\alpha)\dot{q}_{s.s.} - UA_{pc}(T_p - T_c) \\ 0 &= \alpha\dot{q}_{s.s} - UA_{sc}(T_s - T_c) \\ 0 &= UA_{pc}(T_p - T_c) + UA_{sc}(T_s - T_c) - UA_{ch}(T_c - T_{cool,\,in}) \end{aligned} \tag{13}$$

this results in four unknowns: α, T_p, T_c, UA_{pc}. The rest of the parameters are provided in [11] and summarized in Table 5.

Table 5: EMTM Parameters from Datasheet

Parameter	Value
UA_{sc}	18.1818 J/K
UA_{ch}	50.2513 J/K
T_s	140.8 ℃

The value of T_s is the specified temperature of the winding when the motor is operated at its continuous power level. The values of UA_{sc} and UA_{ch} were determined by the inverse of the thermal resistance between the winding and the stator core and the stator core and the coolant.

In steady state operation, all the heat generated must exit through the coolant, so an additional equation can be generated:

$$\dot{q}_{s.s} = UA_{ch}(T_c - T_{cool,\,in}) \tag{14}$$

This results in a system of four nonlinear constrained equations with four unknowns. The constraints on the equation are described by the following:

$$0 \leq \alpha \leq 1; \quad UA_{pc}, T_c, T_p > 0 \tag{15}$$

The distribution of heat, α, must be between 0 and 1, since this is a percentage and the heat transfer coefficient between the rotor and stator core, UA_{pc}, the temperature of the stator core, T_c, and the temperature of the rotor, T_p, all must be greater than zero.

These equations were solved at many different continuous power operating points to generate a lookup table of heat distribution and heat transfer coefficient between the rotor and stator depending on the electric machine rotational speed. As the rotor increases in rotational speed, greater losses are produced in different portions of the motor and the air becomes more turbulent which increases the heat transfer coefficient.

To solve this nonlinear system of equations with constraints, a nonlinear least-squares solver in MATLAB, *lsqnonlin*, was used. The mathematical setup for this optimization is like the setup for the motor controller. This solver gave the following solutions with respect to motor RPM for the parameters:

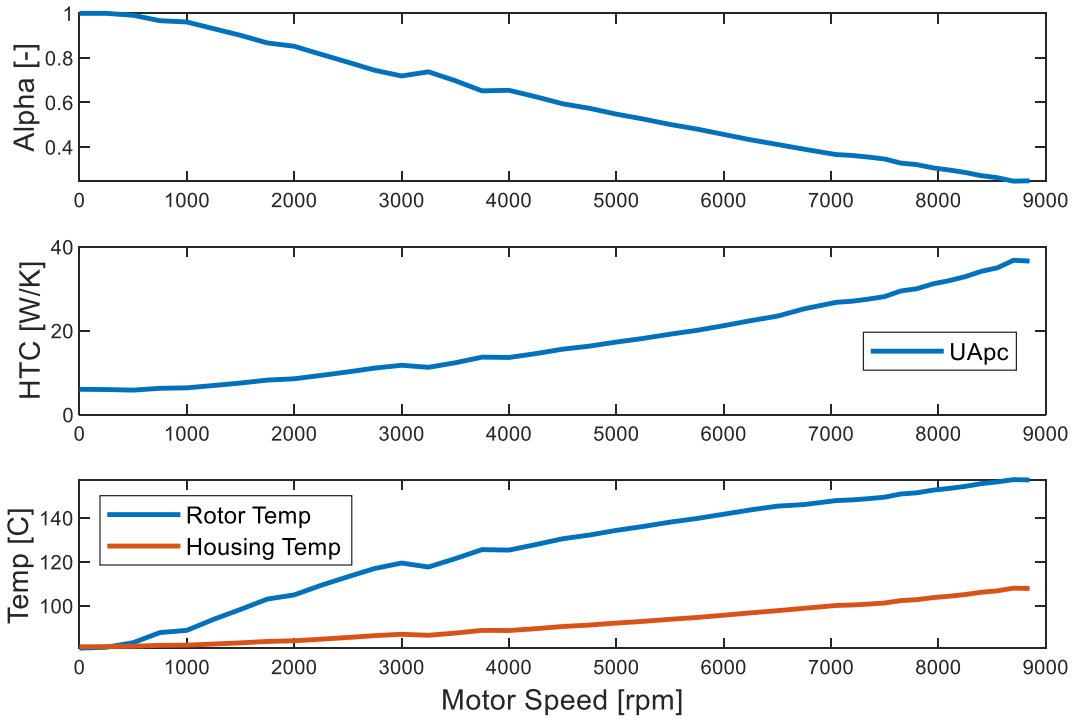

Figure 25: Steady-State Parameter Solutions for Electric Machine

The solution to the steady state equations gave reasonable parameter values. The distribution of heat generation initially starts at 1 then decreases to a minimum of 0.25. This matches expectations as the initially the losses are completely concentrated in the resistance of the copper winding, but as the rotor speed increases additional losses are generated from the friction drag of the bearings on the rotor and eddy currents generated from the rotating permanent magnets. The overall heat transfer coefficient is initially very small as there is little airflow between the rotor and stator core and increases as the rotational speed and turbulence increases. Finally, the values for the rotor temperature and housing temperature are very reasonable considering the known steady state operating temperature of the winding.

The final portion of the electric machine thermal model that must be determined is the transient behavior. The datasheet provided the time constants of the motor winding and the motor housing. These values are listed in Table 6.

Table 6: Time Constants for Electric Machine [11]

Component	Time Constant (min)
Stator Winding	2.5
Stator Core/Motor Housing	9.3

Using these, the values for C_s and C_c can be determined by solving the energy balance of these thermal nodes from Equation 3 for the time constants.

Table 7: EMTM Heat Capacities

Component	Heat Capacity (J/K)
Stator Winding, C_s	2727
Stator Core/Motor Housing, C_c	49000

The last unknown in the thermal model is the time constant for the rotor. This was scaled based on the time constant from a motor presented in literature [8]. The complete electric machine thermal model with all its parameters can be found in Appendix A.

Radiator Calibration

The cooling system data the Buckeye Current team collected in the past that captured the inlet and outlet temperatures of the coolant and the flow rate isn't suitable due to a change in the

radiator placement for RW-4. The differences in the radiator placement is shown in Figures 26 and 27.

Figure 26: RW-3 Radiator Placement

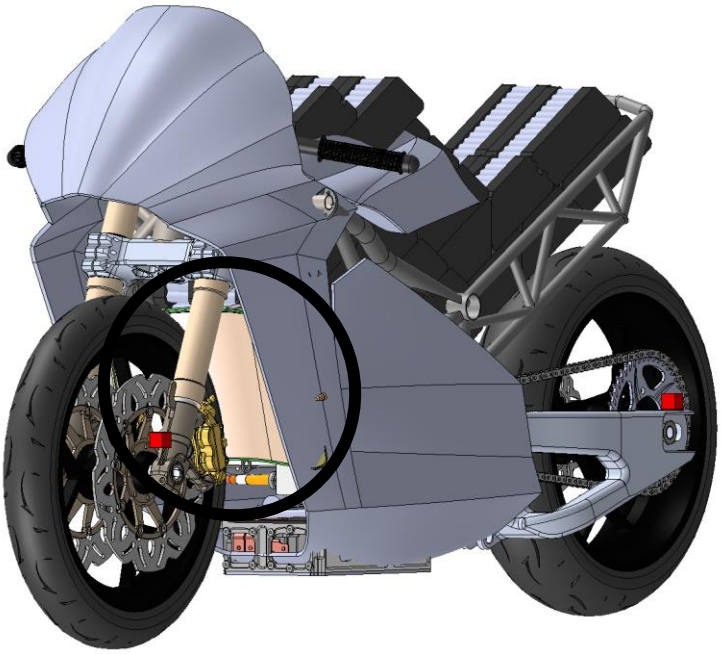

Figure 27: RW-4 Radiator Placement

In RW-3, the radiators were placed below the seat with fans mounted above them. This gave a constant air velocity over the radiators. The constant speed fans provide a very specific operating range and wouldn't provide a range of data to calibrate the radiator model. In RW-4, the radiator is placed in the front of the motorcycle, so the velocity over the radiator varies with vehicle speed. This is the typical radiator position for motorcycles. Most motorcycle manufacturers produce their own radiators, so thermal data is unavailable. Therefore, thermal data for an automotive radiator supplier must be used to tune the model until testing data is available

The supplier data is steady state operating points for the radiator. Therefore, the radiator model described previously by Equation 4 must be simplified to steady state conditions:

$$\dot{Q} = A_f \frac{C_f \dot{m}^{\beta}{}_c}{C_3}\left(T_{c,in} - T_w\right) = A_f \frac{1}{C_2}(T_w - T_s) = A_f \frac{\left(\rho_{air} V_{face}\right)^{\frac{2}{3}}}{C_1}(T_s - T_{air}) \tag{16}$$

where $\dot{Q}$ is the rate of heat transfer through the radiator. This equation can be manipulated to express the heat transfer with respect to $T_{c,in} - T_{air}$:

$$\left(\frac{C_3}{C_f \dot{m}^{\beta}{}_c} + C_2 + \frac{C_1}{\left(\rho_{air} V_{face}\right)^{\frac{2}{3}}}\right) = \frac{A_f}{\dot{Q}}(T_{c,in} - T_{air}) \tag{17}$$

The only unknowns in this equation are the predictors, $C_1, C_2,$ and C_3. These are linear as they are never multiplied by each other.

To solve for these coefficients, the Linear Least Squares method is used:

$$\hat{\pi} = [H^T * H] * H^T * Y \tag{18}$$

where $\hat{\pi}$ is a vector of the parameters, H is a matrix of the measured independent variables, and Y is a vector of the measured dependent variable. For the predictors in the radiator model, these values are defined as follows:

$$\hat{\pi} = \begin{bmatrix} C_3 \\ C_2 \\ C_1 \end{bmatrix} H = \begin{bmatrix} \frac{1}{C_f \dot{m}(1)_c^{\beta}} & 1 & \frac{1}{\left(\rho_{air}(1) V_{face}(1)\right)^{\frac{2}{3}}} \\ \vdots & \vdots & \vdots \\ \frac{1}{C_f \dot{m}(n)_c^{\beta}} & 1 & \frac{1}{\left(\rho_{air}(n) V_{face}(n)\right)^{\frac{2}{3}}} \end{bmatrix} Y = \begin{bmatrix} \frac{A_f}{\dot{Q}(1)} \left(T_{c,in}(1) - T_{air}(1)\right) \\ \vdots \\ \frac{A_f}{\dot{Q}(n)} \left(T_{c,in}(n) - T_{air}(n)\right) \end{bmatrix} \quad (19)$$

where the variables used in H and Y are a subset of the measured data used for calibration of the parameters.

To verify the accuracy of the model, the calibrated model was compared to all available data based on the following variables: exit temperature of the coolant (℃), exit temperature of the air (℃), heat rejection (kW), and effectiveness of the radiator. These variables are defined in the following equations:

$$T_{c,out} = T_{c,in} - \frac{\dot{Q}}{\dot{m}_c c_{p,c}} \quad (20)$$

$$T_{air,out} = T_{air,in} + \frac{\dot{Q}}{\dot{m}_{air} c_{p,air}} \quad (21)$$

$$\epsilon = \frac{T_{air,out} - T_{air,in}}{T_{c,in} - T_{air,in}} \quad (22)$$

The error correlation and statistically distribution of the error for these metrics are shown:

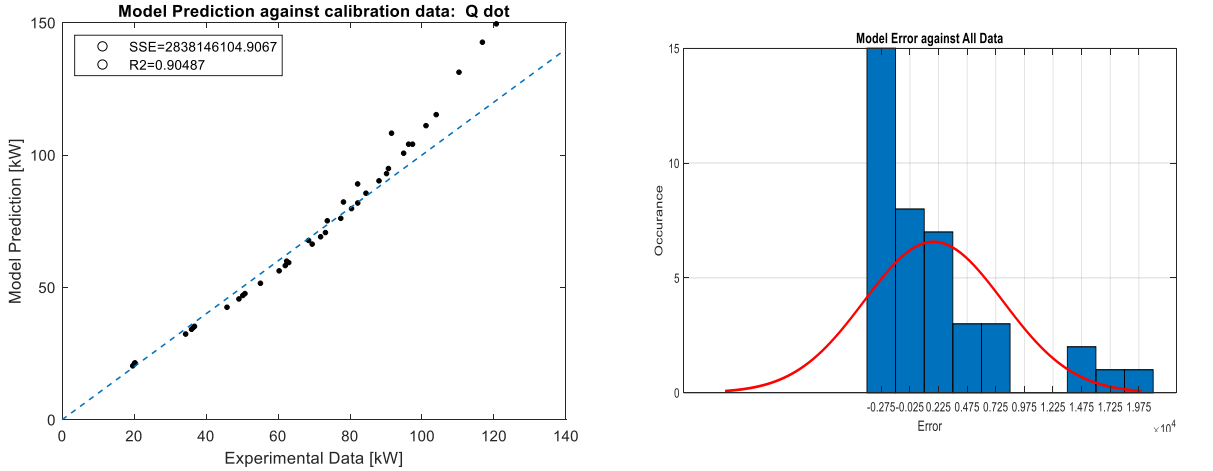

Figure 28: Radiator Error Plots for Heat Rejection

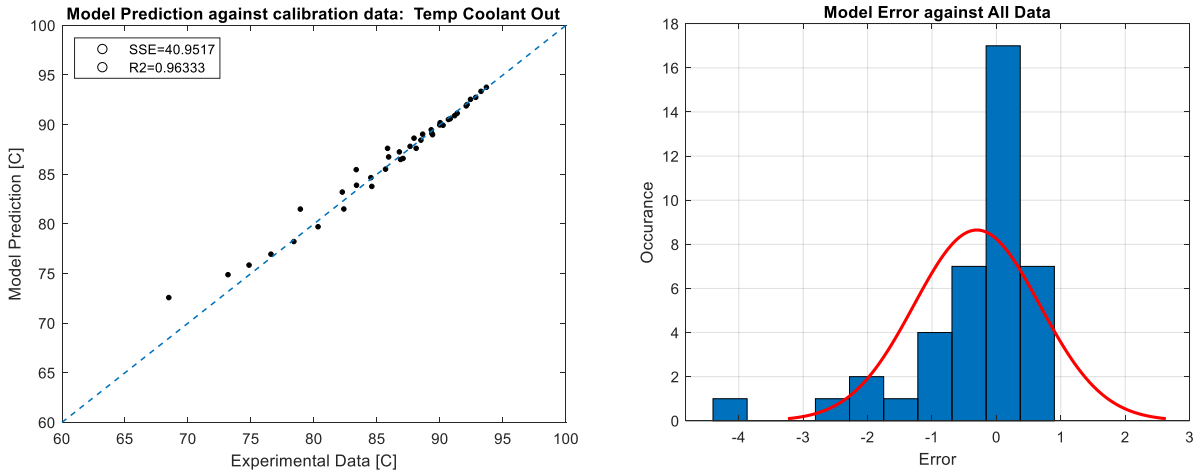

Figure 29: Radiator Error Plots for Coolant Exit Temperature

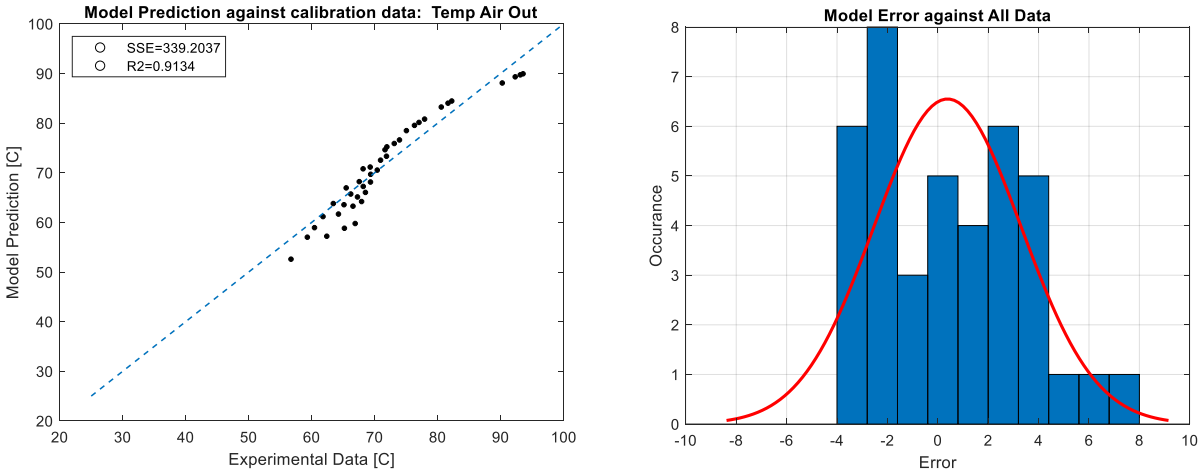

Figure 30: Radiator Error Plots for Air Exit Temperature

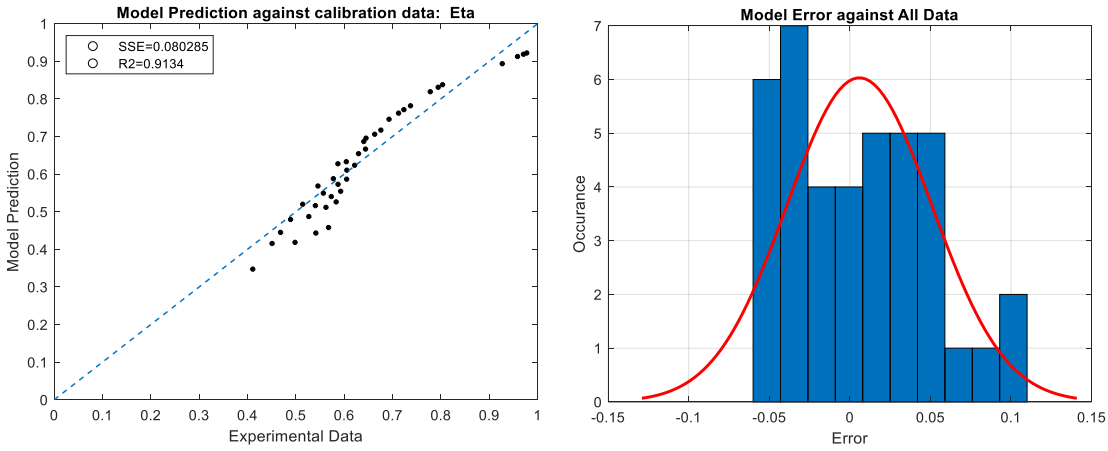

Figure 31: Radiator Error Plots for Eta

The model had the best agreement with the data for the outlet coolant temperature. The error distribution was biased towards the model overestimating the temperature, but the *SSE* is low and the R^2 value is close to 1. The heat rejection was accurate for low heat rejection but the inaccurate at higher heat rejections, where the model overestimated the heat rejection. The exit air temperature appeared to have a slight correlation in the data, but overall had a good fit. Finally, the effectiveness of the radiator shared a similar correlation to the exit air temperature, since it is dependent on this, but again had a decent R^2 value. The fact that the model was most accurate for the coolant exit temperature is important, as this is the most critical of the parameters for the performance of other components in the cooling system.

The predictors, $C_1, C_2,$ and C_3 for the radiator using this data set are listed in Table 8.

.

Table 8: Radiator Predictors

Predictor	**Value [m^2K/W]**
C_1	0.0014
C_2	$1.23 * 10^{-5}$
C_3	0.007

This model has been tuned with high temperature coolant at low face velocities compared to a motorcycle radiator. To verify the performance of the radiator model, inlet and outlet temperature data collected from PPIHC for the motor controller was used, along with scaling the radiator to the appropriate size and setting a constant face velocity, which the radiators on RW-3 saw from the fans mounted in the tail. The outlet temperature data from the radiator on RW-3 was collected from within the coolant reservoir, so the radiator and reservoir models were combined to test the performance compared to experimental data. These results are shown in Figure 32.

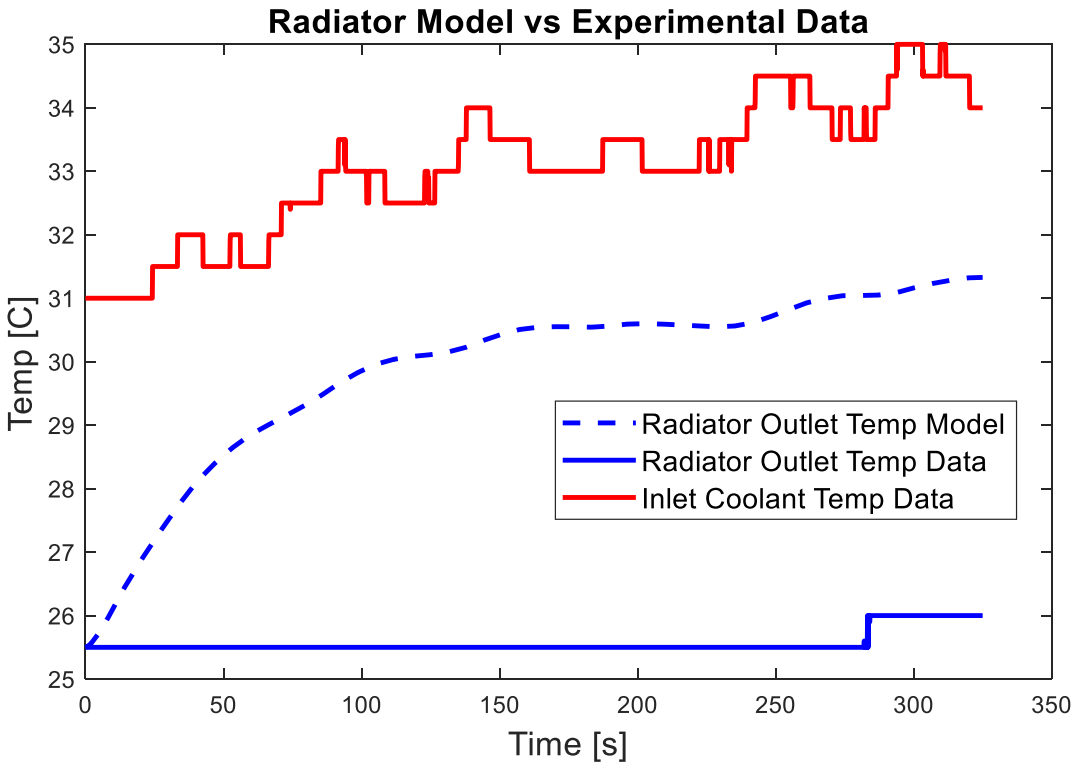

Figure 32: Radiator and Reservoir Validation

Large errors were seen between the model projected temperature and the measured temperature. These errors are likely due to errors in the data collection process. The temperature sensor used in RW-3 had a long time constant and was inaccurate at ambient temperatures [13]. To prevent these limitations for RW-4, an appropriate temperature sensor has been chosen. These temperature measurements would also lead to errors in the motor controller thermal model as the true inlet coolant temperature for this model was likely greater than the data suggested. However, if the true inlet coolant temperature was used to calibrate the model, then to maintain the same heat rejection, the heat transfer coefficient between the coolant and the motor controller would need to be greater. Therefore, this error leads to the model being slightly conservative and underestimating the heat rejection.

To validate the radiator model, additional data will need to be collected from testing with RW-4. However, the heat rejection from the Buckeye Current electric motorcycle is significantly less than for a typical ICE motorcycle, and because the radiator is sized for this higher heat rejection, it should be adequately sized. The complete radiator model with all its parameters can be found in Appendix A.

Chapter 5: Design Optimization

Buckeye Current's Simulation Tools

To predict motorcycle performance, Buckeye Current uses a point-mass, longitudinal vehicle simulator that attempts to follow an ideal velocity profile while subject to physical limitations such as aerodynamic drag, rolling resistance, and elevation changes. By simulating the motorcycle's performance with specific powertrain components, the team can determine energy requirements, estimated lap time, and aerodynamic requirements. The development of this tool is outside the scope of this work, but it provides a current and power demand profile for the electric machine, the DC bus voltage and motor RMS current for the heat rejection in the motor controller, and face velocity for the radiator. Therefore, the thermal models that have been developed in this work can be integrated into this simulation tool to predict the temperature rise of these components during the race. The thermal model of the motor controller has been tested against data not used in the calibration process and predicted the temperatures accurately. No thermal data is available to validate the electric machine or radiator thermal models. This data will need to be collected during testing of RW-4. With these limitations, the thermal models can be used as a guide to suggest trends in the temperatures of the components and once data is collected by the Buckeye Current team and the models are validated, they can be used for more detailed control strategy design and race performance prediction.

Cooling System Design

The thermal models of the components were implemented in Simulink and then added to the vehicle simulation. To determine the requirements for RW-4's cooling system, a variety of cooling system configurations must be evaluated. The potential configurations are either a single

loop cooling system with the electric machine first or the motor controller first, or separate cooling loops for both the electric machine and the motor controller. A single cooling loop would reduce complexity of the cooling system design, so this is the preferred arrangement. The required flow rate from the electric machine and motor controller datasheet was specified at 8-10 LPM. To reduce the change in coolant temperature and maximize convection between the components and coolant, a 10 LPM flow rate will be used. Finally, alternative initial conditions and powertrain control strategies will be explored to determine the effect that power reduction has on the trends in component temperatures.

The combined cooling circuit was tested with both possible configurations, motor controller first and then electric machine first. Diagrams depicting the flow of coolant through these two configurations are shown in Figure 33. For optimal thermal performance, the electric machine and motor controller were prechilled to 0 ℃. The initial temperature of the coolant, which is pure water, was set to 3 ℃. With these initial conditions, the predicted performance for the motor controller, electric machine, and radiator for each configuration is shown in Figures 34 and 35.

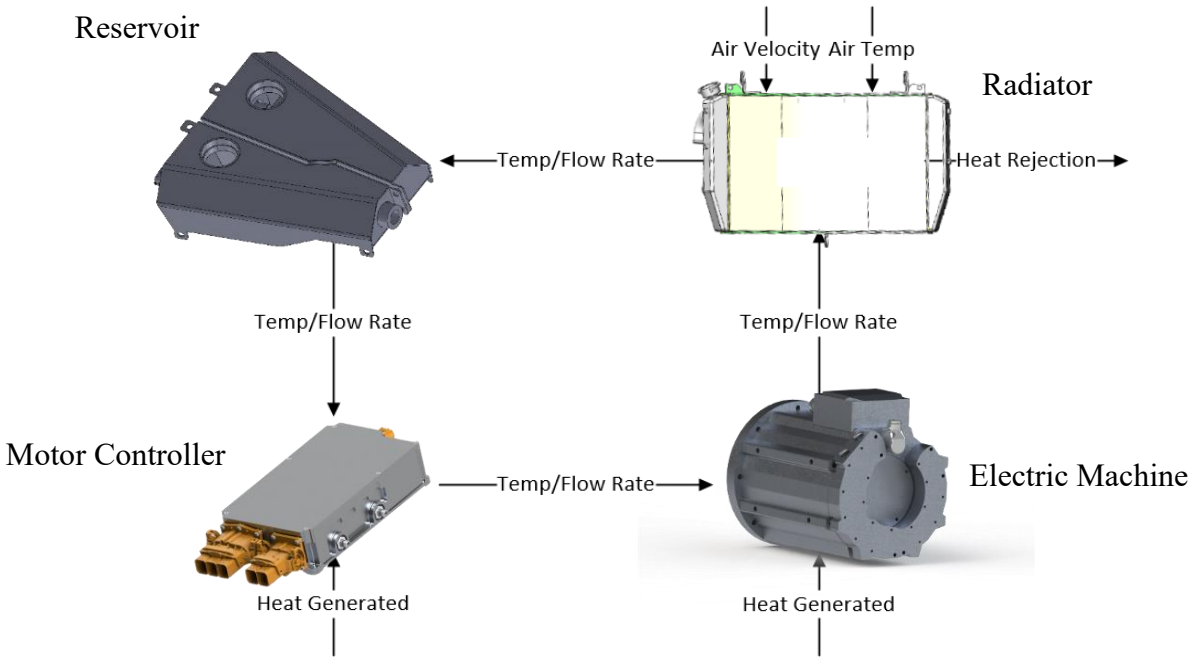

(a)

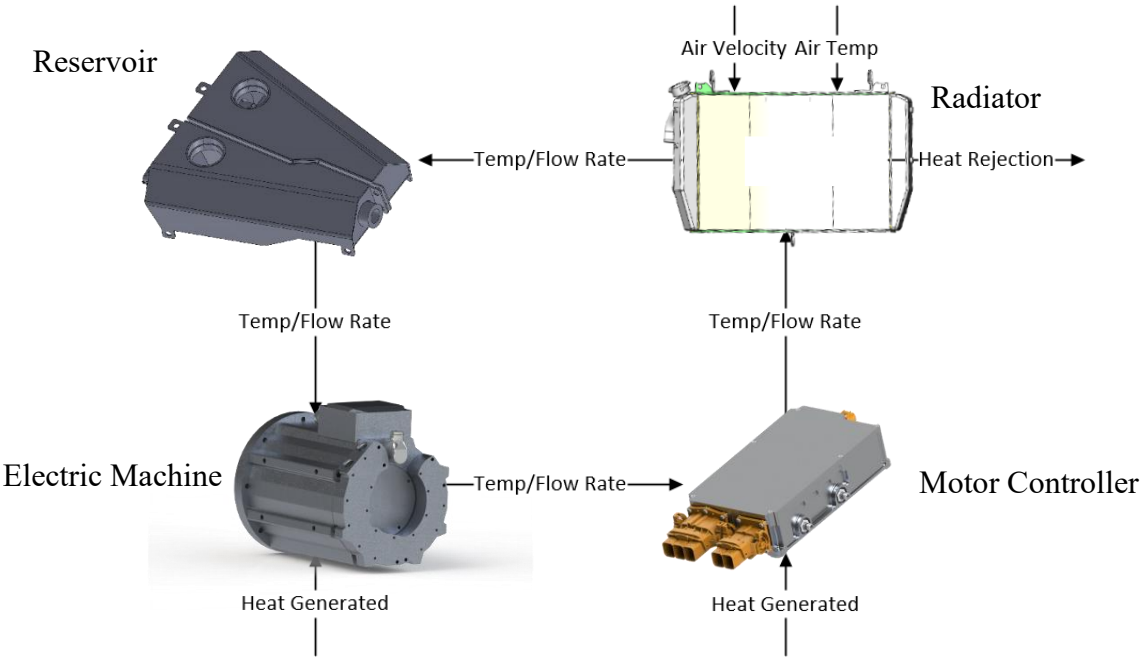

(b)

Figure 33: Combined Cooling Loop (a) Motor Controller First (b) Electric Machine First

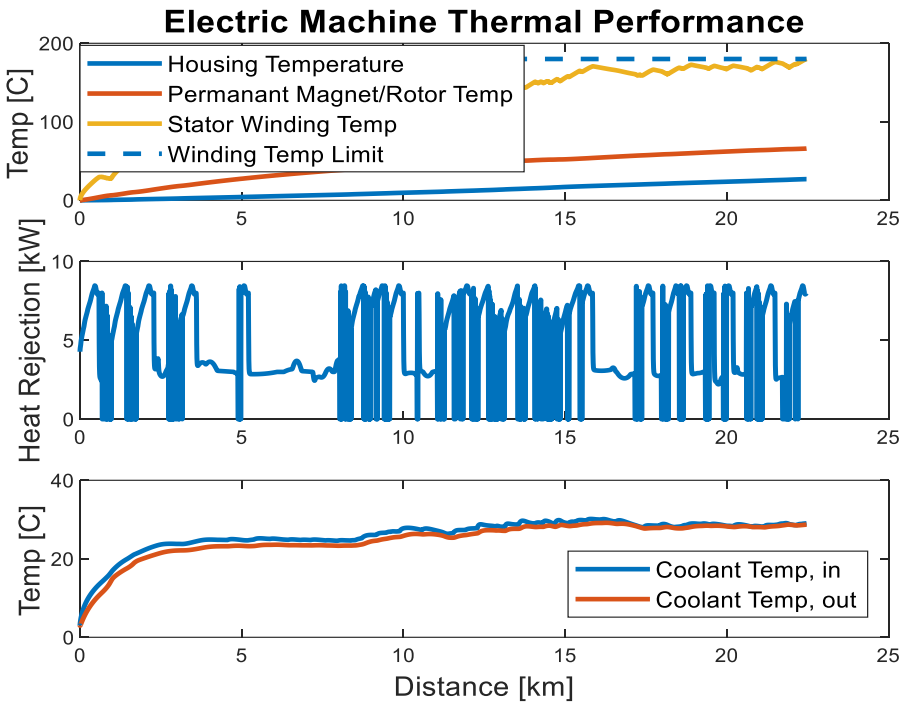

(a)

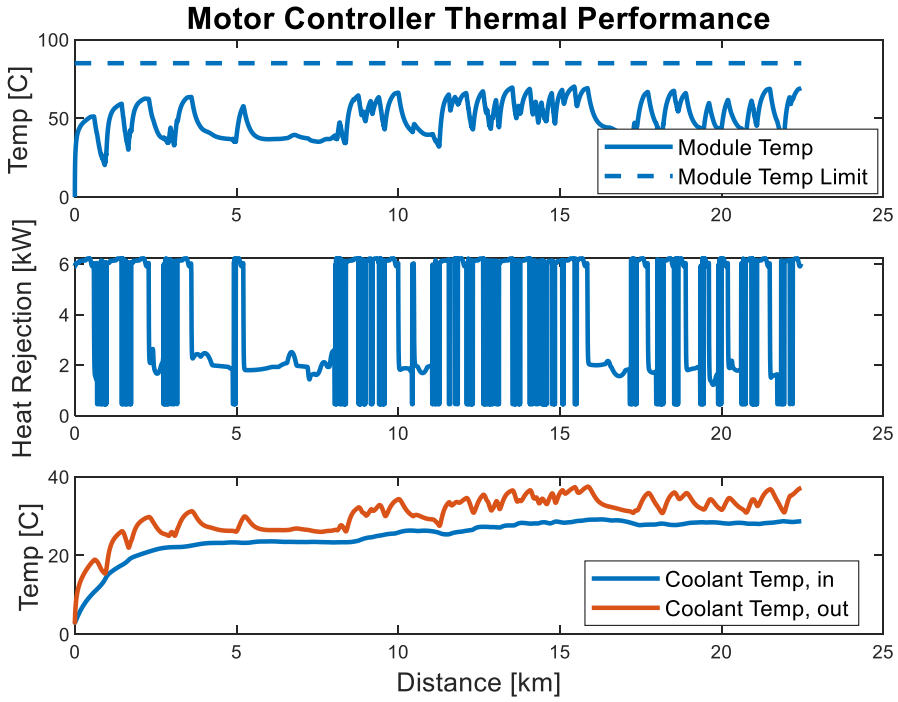

(b)

Figure 34: Combined Loop, Electric Machine First (a) Electric Machine Thermal Performance (b) Motor Controller Thermal Performance

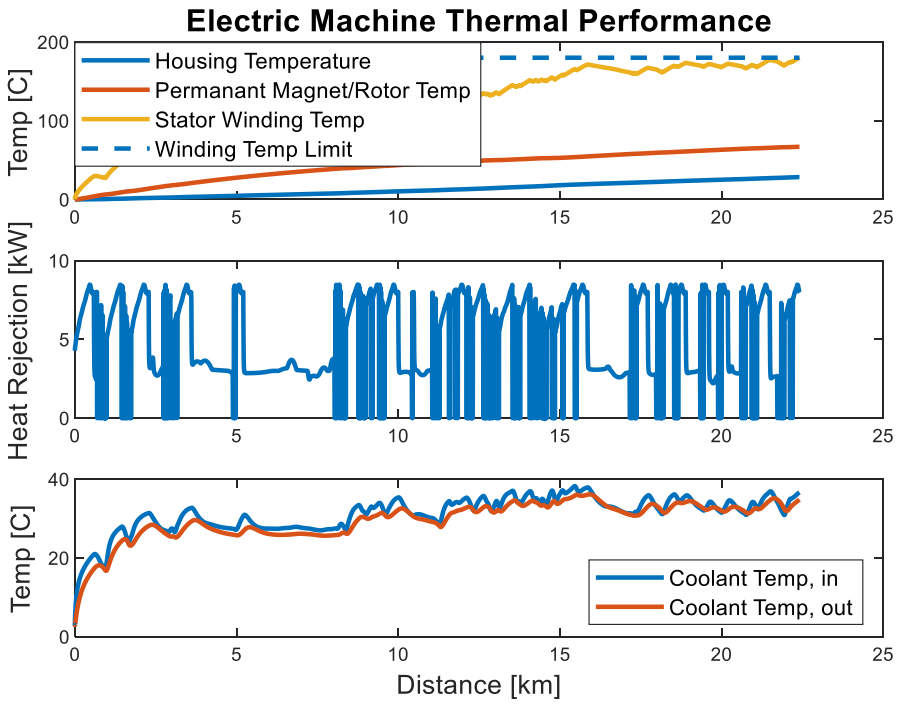

(a)

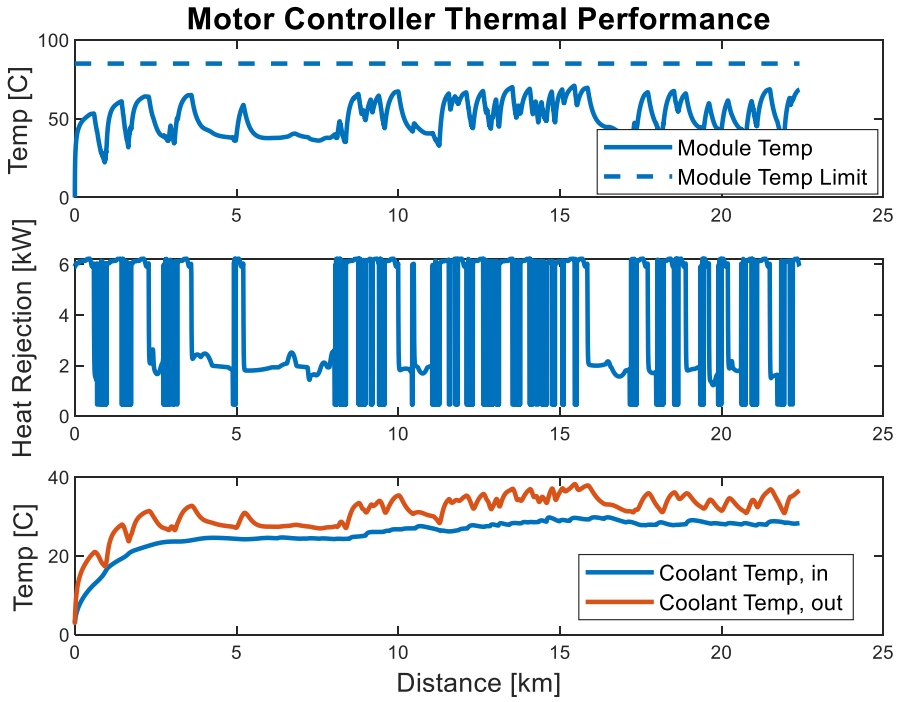

(b)

Figure 35: Combined Loop, Motor Controller First (a) Electric Machine Thermal Performance (b) Motor Controller Thermal Performance

In both combined loop configurations, the electric machine exceeds it maximum operating temperature while the motor controller does not reach the recommended thermal limitation, 85 ℃. Therefore, a combined cooling system is feasible with the motor first to reduce thermal limitations. The projected stator winding temperatures of the electric machine quickly increases as the power level the machine is operating greatly exceeds its continuous power rating, but thermal data from dynamometer testing will determine if these projected temperatures are reasonable.

The large time constant for the electric machine stator core and housing prevent significant heat rejection to the coolant, particularly at the beginning of operation when both temperatures are near ambient. Also, the large amount of heat generation in the windings cause their temperature to increase and projects them to exceed the maximum allowable operating temperature, 180 ℃. To prevent the motor from exceeding this temperature,

While operating at full power, the motor reached its maximum allowable operating temperature prior to completing the race. The maximum temperature was exceeded after 22,500 meters had been traveled while the Isle of Man circuit is approximately 60,000 meters long. Therefore, power limiting control strategies were explored to determine the magnitude of their effect on thermal performance. The percentage of maximum power allowed was reduced using the low initial temperature cooling conditions until the winding of the electric machine remained below its maximum allowable operating temperature for the entirety of the race. The electric machine was limited to producing 80% of the maximum torque possible to reduce losses. The change in operating points from this control strategy is shown in Figure 36 while the thermal performance of the powertrain is shown in Figure 37.

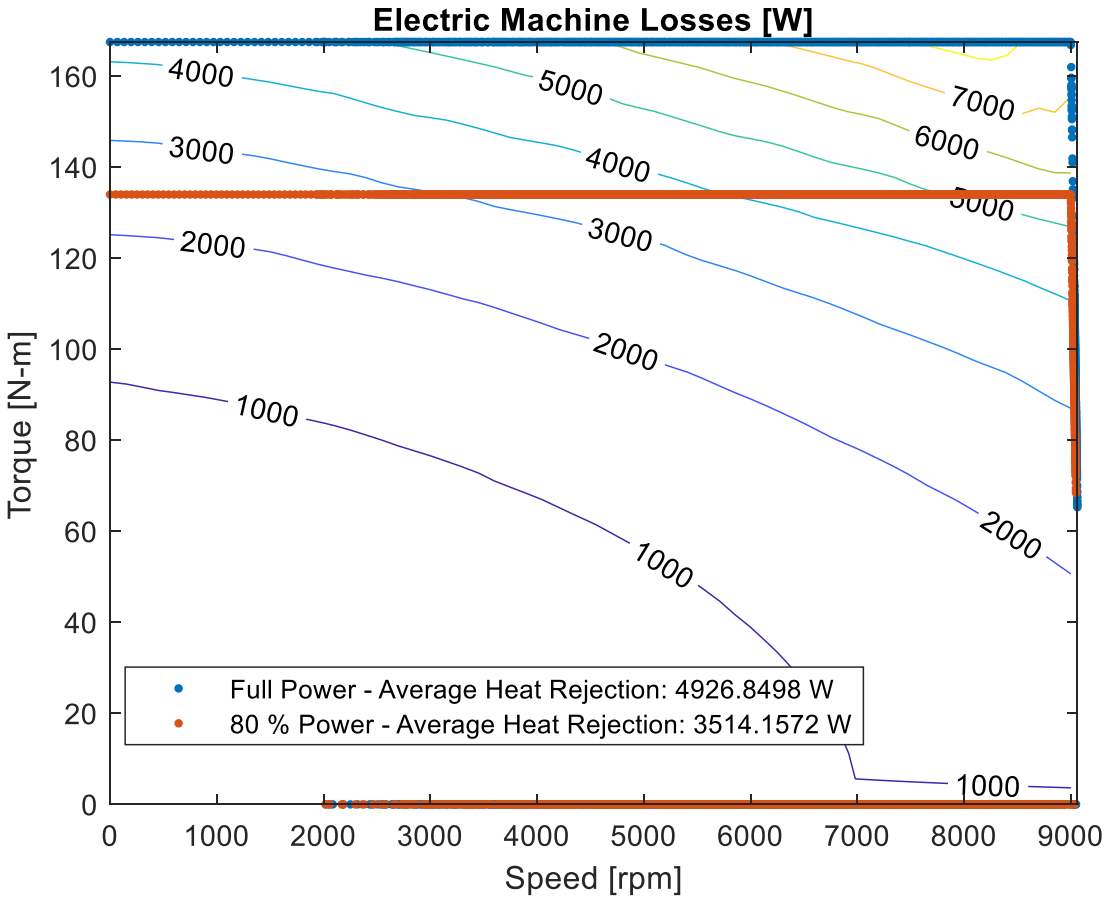

Figure 36: Electric Machine Power Limiting Strategy

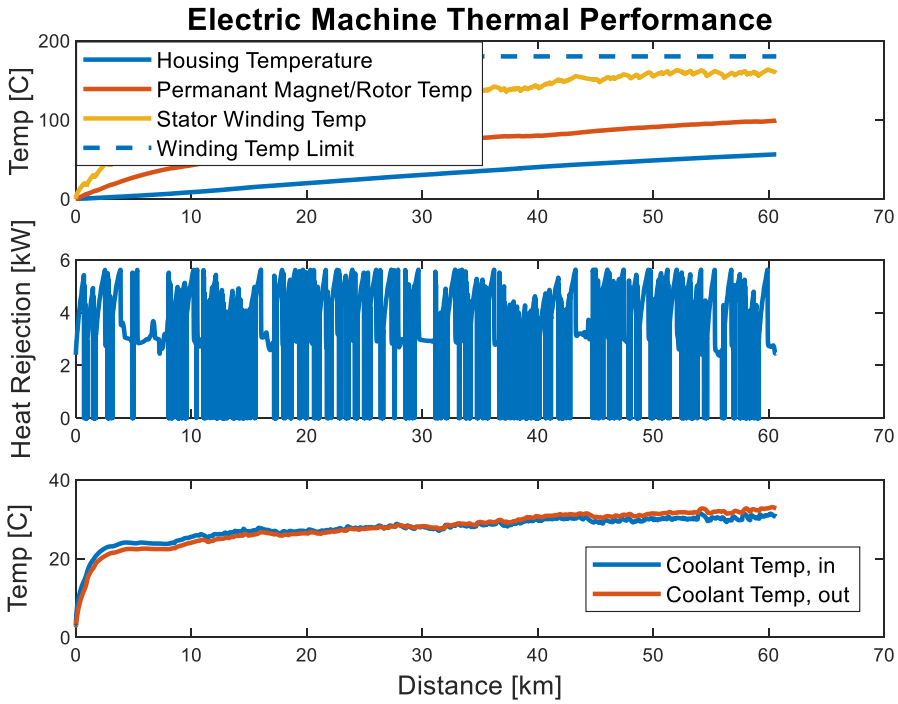

(a)

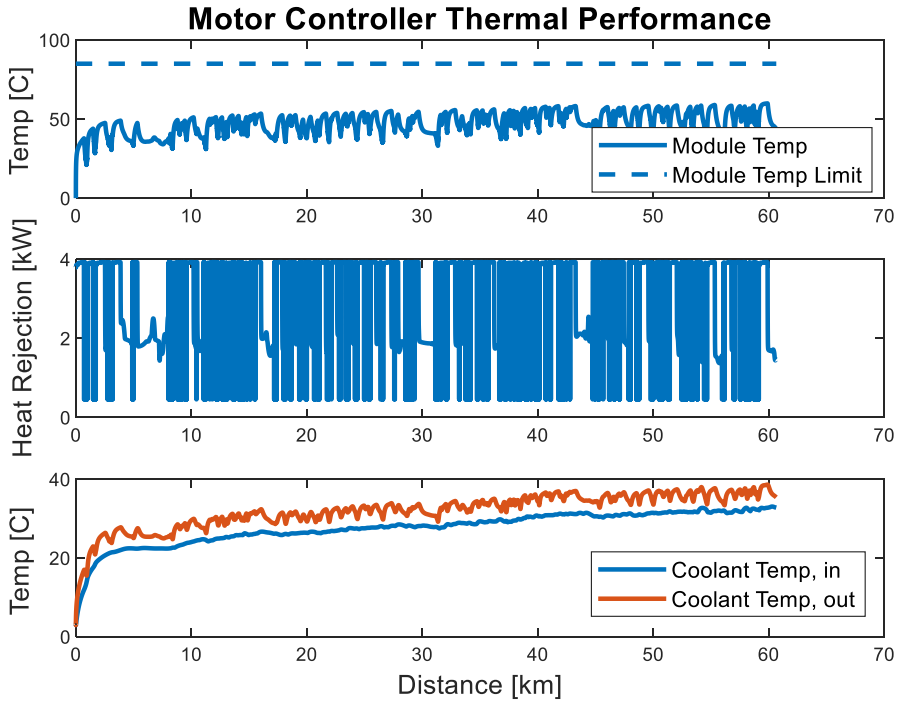

(b)

Figure 37: Limited Combined Loop, Electric Machine First (a) Electric Machine Thermal Performance (b) Motor Controller Thermal Performance

By limited power to 80% of the maximum and starting with a prechilled cooling system, the maximum temperature the windings of the electric machine is significantly reduced. This occurs as the electric machine produces less heat at lower torques and speeds.

By reducing power 20%, the average heat rejection of the electric machine is reduced by 29%. Also, with the current electric machine thermal model, most of these additional losses from operating at maximum power are concentrated in the stator windings, which leads to them reach extremely high temperatures due to the small thermal mass. This assumption for the thermal model must be validated with testing, then the heat rejection map can be used to determine an ideal control strategy.

Based on this analysis, the Buckeye Current team should prechill the cooling system, particularly the housing of the electric machine, and limit power during the race. Greater control strategies for power limitation can be created once additional thermal data are collected and the models are validated. Prechilling the motor housing appears to make the coolant entering and leaving the motor have virtually no effect as much of the heat is stored in the large thermal mass in the casing. However, the heat rejection within the motor controller relies heavily on the coolant as there is no similar large thermal mass, so the recommended flow rate should be maintained.

Chapter 6: Conclusion

In this thesis, physics based thermal models were created for an electrified powertrain. These include the electric machine, the motor controller, the radiator, and the reservoir. These models were tuned using data the Buckeye Current team collect at PPIHC in 2017 and information from datasheets. With these thermal models, the thermal system of Buckeye Current's electric motorcycle was analyzed for the operating conditions at the Isle of Man TT Zero. The temperature trends of these key components and requirements for the cooling system along with control strategies for the electric machine to prevent these components from exceeding their maximum operating temperature were explored. Based on this analysis, the Buckeye Current team can design an optimized cooling system for their new electric motorcycle RW-4.

This work had many innovations for modeling of an electrified powertrain's cooling system. A single node, accurate motor controller thermal model was created to predict the temperature of the switching modules. Also, a process for tuning a simplified thermal model of an electric machine using only information available from a supplier's datasheet was created. However, testing data is still required to verify the performance of the thermal model. Finally, the process of analyzing the cooling system for an electrified powertrain, including the cooling system configuration options, alternative initial conditions, and power limitations, was outlined.

This thesis provided a strong starting point for cooling system analysis, however, limitations in available data forced creative methods for tuning the parameters of the electric machine and radiator thermal models. Once the Buckeye Current team receives the electric machine, dynamometer testing can be performed to collect thermal data that can be used to

validate the thermal model and retune the model parameters. Also, the radiators used on motorcycles differ from cars due to the high face velocities and turbulence caused by the spinning front wheel. Once a prototype for RW-4 has been built, inlet and outlet temperature data and face velocity can be used to validate or retune the radiator model at the operating conditions of a motorcycle. Finally, the control strategy suggested for the electric machine in this thesis was a uniform power reduction. However, the operating efficiency of the machine varies depending on its operating conditions. By using the machine's efficiency map and feedback from the rider on where in the circuit extra power is needed, the team can vary the power available from the machine to maximize the motorcycle's performance. With additional data, the Buckeye Current team will have a reliable model of their thermal system and can design their control strategy to prevent the powertrain from exceeding its maximum operating temperature during the Isle of Man TT Zero race.

References

[1] The University of Michigan Sustainable Worldwide Transportation, Report No. SWT-2017- 18 November 2017

[2] The official U.S. government source for fuel economy information. (n.d.). Retrieved from https://www.fueleconomy.gov/

[3] White, L. V., & Sintov, N. D. (2017). You are what you drive: Environmentalist and social innovator symbolism drives electric vehicle adoption intentions. *Transportation Research Part A: Policy and Practice,99*, 94-113. doi:10.1016/j.tra.2017.03.008

[4] Hall, T. J. (2017). An Analysis of Braking Behavior in Formula-E® Racing. *SAE Technical Paper Series*. doi:10.4271/2017-01-2533

[5] Theodore L. Bergman; Adrienne S. Lavine; Frank P. Incropera; David P. DeWitt. *Fundamentals of Heat and Mass Transfer*, 8th Edition. Wiley. Kindle Edition.

[6] Abdelli, A. (2014). Optimal Design of an Interior Permanent Magnet Synchronous Motor for Wide Constant-Power Region Operation: Considering Thermal and Electromagnetic Aspects. *SAE International Journal of Alternative Powertrains,3*(1), 129-138. doi:10.4271/2014-01-1889

[7] Chaieb, M., Hadj, N. B., Kammoun, J., & Neji, R. (2014). Thermal modeling of permanent magnet motor with finite element method. *2014 15th International Conference on Sciences and Techniques of Automatic Control and Computer Engineering (STA)*. doi:10.1109/sta.2014.7086733

[8] Kral, C., Haumer, A., & Lee, S. B. (2014). A Practical Thermal Model for the Estimation of Permanent Magnet and Stator Winding Temperatures. *IEEE Transactions on Power Electronics,29*(1), 455-464. doi:10.1109/tpel.2013.2253128

[9] Ustun, O., Cakan, M., Tuncay, R. N., Mokukcu, M. S., Kivanc, O. C., Mutlu, Y., & Tosun, G. (2014). Design and manufacture of electric powertrain and its cooling system for ITU EV project. *2014 International Conference on Electrical Machines (ICEM)*. doi:10.1109/icelmach.2014.6960262

[10] Scott, T., *"Modeling Compact Exchangers for HVAC Applications",* ASME Summer Heat Transfer Conference, July 2003.

[11] Agarwal, N., Chiara, F., & Canova, M. (2012). Control-Oriented Modeling of an Automotive Thermal Management System. *IFAC Proceedings Volumes,45*(30), 392-399. doi:10.3182/20121023-3-fr-4025.00051

[12] Parker, GVM 210-100 P6 datasheet, Jan. 2019

[13] Bosch Motorsport, NTC M12-H datasheet, Jan. 2019

Appendix A:

Motor Controller Thermal Model

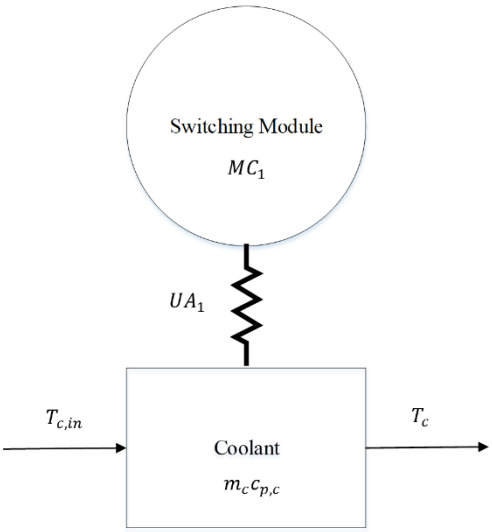

Heat Rejection (Watts):

$$\dot{Q}_{heat} = 0.000244 * {V_{DC}}^{1.072} * {I_{RMS}}^{1.695} + 456.4$$

Switching Module Node:

$$MC_1 \frac{dT_1}{dt} = \dot{Q}_{heat} - UA_1(T_1 - T_{c,in})$$

Coolant:

$$m_c c_{p,c} \frac{dT_c}{dt} = \dot{m}_c c_{p,c}(T_{c,in} - T_c) + UA_1(T_1 - T_{c,in})$$

Model Inputs: Coolant inlet temperature, Coolant flow rate, heat generation

Model Outputs: Coolant outlet temperature, Switching module temperature

Parameter	Value
MC_1	363.2 J/K
UA_1	143.9 W/K
m_c	0.1995 kg

Electric Machine Thermal Model

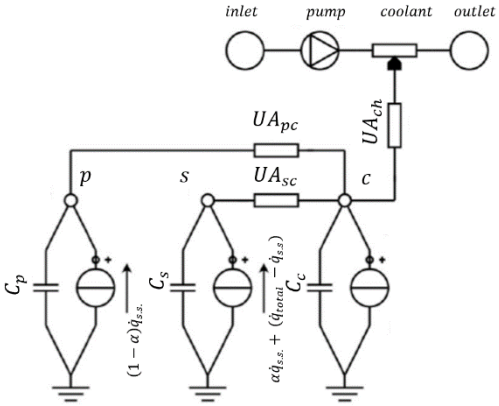

Permanent Magnet (Rotor) Node:

$$M_p C_p \frac{dT_p}{dt} = (1-\alpha)\dot{q}_{s.s.} - UA_{pc}(T_p - T_c)$$

Stator Winding Node:

$$M_s C_s \frac{dT_s}{dt} = \alpha\dot{q}_{s.s} - UA_{sc}(T_s - T_c) + (\dot{q}_{total} - \dot{q}_{s.s})$$

Stator Core/Housing Node:

$$M_c C_c \frac{dT_c}{dt} = UA_{pc}(T_p - T_c) + UA_{sc}(T_s - T_c) - UA_{ch}(T_c - T_{cool,\,in})$$

Model Inputs: Coolant inlet temperature, coolant flow rate, total heat generation (efficiency), continuous power heat generation (efficiency at continuous power rating), rotor to stator core heat transfer coefficient, and alpha at operating RPM, coolant specific heat

Model Outputs: Coolant outlet temperature, rotor temperature, stator winding temperature, stator core temperature

Parameter	Value
$M_p C_p$	7646 J/K
$M_s C_s$	2727 J/K
$M_c C_c$	49000 J/K
UA_{sc}	18.18 W/K
UA_{ch}	50.25 W/K

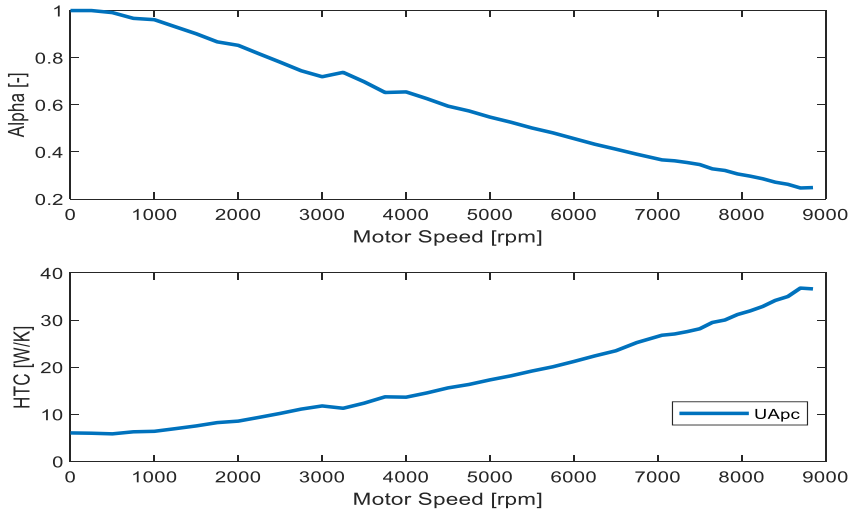

Radiator Thermal Model

Coolant Control Volume:

$$C_c \frac{dT_c}{dt} = \dot{m}_c c_{p,c}\left(T_{c,in} - T_c\right) - A_f * \frac{C_f \dot{m}_c^{\beta}}{C_3}(T_c - T_w)$$

Wall Thermal Mass:

$$C_w \frac{dT_w}{dt} = A_f * \frac{C_f \dot{m}_c^{\beta}}{C_3}(T_c - T_w) - A_f \frac{1}{C_2}(T_w - T_s)$$

Fins and External Surface Mass:

$$C_s \frac{dT_s}{dt} = A_f \frac{1}{C_2}(T_w - T_s) - A_f \frac{\left(\rho_{air} V_{face}\right)^{\frac{2}{3}}}{C_1}(T_s - T_{air})$$

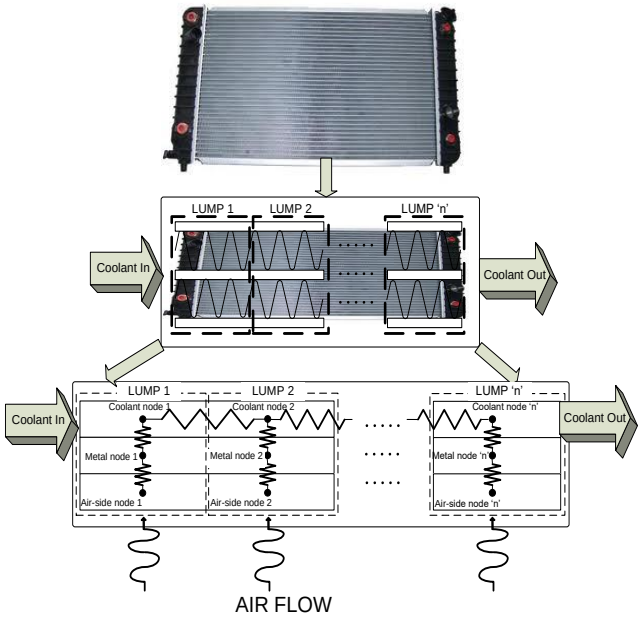

Model Inputs: Coolant inlet temperature, coolant flow rate, air temperature, face velocity, air density, coolant specific heat

Model Outputs: Coolant outlet temperature, wall temperature, fins temperature

Parameter	Value
C_c	1767 J/K
C_w	6.843 J/K
C_s	3914 J/K
C_f	206.9
β	0.8
A_f	0.088 m^2
C_1	0.0014
C_2	1.23e-5
C_3	0.007